Scholar Commons
USF University of South Florida

University of South Florida
Scholar Commons

Graduate Theses and Dissertations

Graduate School

March 2019

Power Conditioning System on a Micro-Grid System

Tamoghna Banerjee
University of South Florida, tamoghna99@yahoo.com

Follow this and additional works at: https://scholarcommons.usf.edu/etd

Part of the Electrical and Computer Engineering Commons

Scholar Commons Citation
Banerjee, Tamoghna, "Power Conditioning System on a Micro-Grid System" (2019). *Graduate Theses and Dissertations.*
https://scholarcommons.usf.edu/etd/7736

This Thesis is brought to you for free and open access by the Graduate School at Scholar Commons. It has been accepted for inclusion in Graduate Theses and Dissertations by an authorized administrator of Scholar Commons. For more information, please contact scholarcommons@usf.edu.

www.manaraa.com

Power Conditioning System on a Micro-Grid

System

by

Tamoghna Banerjee

A thesis submitted in partial fulfillment
of the requirements for the degree of
Master of Science in Electrical Engineering
Department of Electrical Engineering
College of Engineering
University of South Florida

Major Professor: Wilfrido Moreno, Ph.D.
Chung Seop Jeong, Ph.D.
Ashwin Parthasarathy, Ph.D.

Date of Approval:
March 19, 2019

Keywords: Photovoltaic Cell, Fuel Cell, DFIG, PI
Controllers, Inverter

Copyright © 2019, Tamoghna Banerjee

www.manaraa.com

DEDICATION

This thesis is dedicated to my parents. They have provided me ample support to complete my graduate studies. I also dedicate this project to my sibling, for she has motivated me to move on when faced with a roadblock. Lastly, I want to dedicate my committee professors to support my work and providing me food for thought.

www.manaraa.com

ACKNOWLEDGMENTS

I would like to acknowledge my committee members for motivating me and providing me support in making this thesis a success. I would like to thank the College of Engineering for their services. Lastly, I would also like to thank USF Library services for providing me with materials for this topic.

www.manaraa.com

TABLE OF CONTENTS

LIST OF TABLES iii

LIST OF FIGURES iv

ABSTRACT vi

CHAPTER 1: INTRODUCTION 1

CHAPTER 2: WIND GENERATOR 2
2.1 Converter Control 6
2.1.1 Grid-Side Converter (GSC) Control 7
2.1.1.1 Outer Loop Control 8
2.1.1.2 Inner Loop Control 8
2.1.2 Rotor-Side Converter (RSC) Control 10
2.1.2.1 Outer Loop Control 10
2.1.2.2 Inner Loop Control 10
2.1.3 DC-Link 12
2.2 Wind Turbine 12
2.3 Doubly-fed Induction Generator 12
2.4 Shaft System 14

CHAPTER 3: PHOTOVOLTAIC CELL 16
3.1 Basics of Photovoltaic (PV) Cell 16
3.2 Step-Up Converter 17
3.3 Maximum Power Point Tracking 18
3.3.1 Fixed Voltage Method 18
3.3.2 Fractional Open Circuit Method 19
3.3.3 Perturb and Observe Method 19
3.3.4 Incremental Conductance Method 20

CHAPTER 4: FUEL CELL 24
4.1 Introduction to Fuel Cell 24
4.2 Power Electronics Circuit for Fuel Cell 24
4.2.1 Control Logic 24
4.2.2 DC-DC Converter 25

CHAPTER 5: THREE-PHASE INVERTER 26
5.1 Introduction 26

www.manaraa.com

5.2 Pulse Width Modulation Switching Scheme 27

CHAPTER 6: ZERO ORDER HOLD 29

CHAPTER 7: MATLAB BLOCKS 31
7.1 Memory 31
7.2 Tags 31
7.3 Switch 32
7.4 First-Order Filter 33
7.5 Second-Order Filter 34

CHAPTER 8: 13-BUS DISTRIBUTION FEEDER 36

CHAPTER 9: RESULTS 37

CHAPTER 10: CONCLUSION 42

REFERENCES 44

APPENDIX A: RATING OF SYSTEM 46

www.manaraa.com

LIST OF TABLES

Table A.1 Rating of Doubly Fed Induction Generator..... 46

Table A.2 Rating of a PV Array 47

Table A.3 Rating of a Battery.....47

www.manaraa.com

LIST OF FIGURES

Figure 2.1 Type-1 Wind Turbine 2

Figure 2.2 Type-2 Wind Turbine 3

Figure 2.3 Type-3 Wind Turbine 4

Figure 2.4 Type-4 Wind Turbine 5

Figure 2.5 Simulation Model of Doubly Fed Induction Generator 6

Figure 2.6 Control Block of Grid Side Converter 7

Figure 2.7 Subsystem Block of Grid Side Converter 9

Figure 2.8 Control Block Diagram of Rotor Side Converter 10

Figure 2.9 Subsystem Block Diagram of Rotor Side Converter 11

Figure 2.10 State Space Model of Doubly Fed Induction Generator 13

Figure 2.11 Simulation Model of Torque Calculations 15

Figure 3.1 Simulation Model of Photovoltaic System 16

Figure 3.2 Simulation Model of Step-Up Converter 17

Figure 3.3 Algorithm of Maximum Power Point Tracking 21

Figure 3.4 Graph of Maximum Power Point Tracking 22

Figure 3.5 Simulation Model of Maximum Power Point Tracking 22

Figure 3.6 Switching Pulse 23

Figure 4.1 Simulation Model of Control Block 24

Figure 4.2 Switching Pulse 25

www.manaraa.com

Figure 4.3 Simulation Model of Fuel Cell Circuit 25
Figure 5.1 Simulation Model of Three-Phase Inverter 26
Figure 5.2 Simulation Model of Sinusoidal PWM 27
Figure 5.3 Graph of Sinusoidal PWM 28
Figure 6.1 Zero Order Hold Block 29
Figure 6.2 Zero Order Hold Graph 29
Figure 7.1 Memory Block 31
Figure 7.2 From Tag 32
Figure 7.3 Goto Tag 32
Figure 7.4 Switch Block 33
Figure 7.5 First-Order Filter Block 34
Figure 7.6 Second-Order Filter Block 35
Figure 8.1 13 Bus Radial Network 36
Figure 9.1 Circuit Diagram of Simulink Model 37
Figure 9.2 Output from Photovoltaic Cell 38
Figure 9.3 Output from Battery System 38
Figure 9.4 DC Output 39
Figure 9.5 Three-Phase AC Output 39
Figure 9.6 Flow of Active and Reactive Power 40
Figure 9.7 Stator and Rotor Current 40
Figure 9.8 DFIG Angular Speed 41
Figure 9.9 Torque 41
Figure 10.1 Three-Phase AC Output 43

www.manaraa.com

ABSTRACT

This paper presents renewable energy, power electronics, and distributed generators. The focus is on wind farm generator, photovoltaic cell, and battery bank system. Power Conditioning system improves the performance of a power system. Apart from the benefits of converting between DC/AC, there is adequate control of real power and additional control of economic reactive power. This is possible because of multiple sources in the system.

This project throws light on the basic principle of power system conditioning, its operation and control, and the economic studies.

www.manaraa.com

CHAPTER 1: INTRODUCTION

Distributed generations increase the efficiency of the system. Hence there is an increased demand for renewable resources. They support sustainable development and the global economy. They are increasingly attractive, as they can solve global environmental pollution and energy shortage. Among the renewable energy, a wind generator and the photovoltaic cell is high in demand. The major disadvantage of photovoltaics is the high generation cost and the high cost of the devices. The disadvantage of wind farm generator that it has expensive design cost and design issues may result in lower reliability. Apart from the drawbacks, power generations using renewables have high efficiency, fast response, design flexibility, and low environmental effect.

Wind-farm generators using a doubly-fed induction generator (DFIG) have several advantages. It comes with flexible control for active and reactive power, reduced cost for converters and low power loss. A DFIG has two sides: grid-side and rotor-side. The grid-side is connected from the stator terminal to the power grid. The rotor-side connected from rotor terminals via AC/DC/AC converter to power grid. During variable wind speed, the back-to-back converters connected between the rotor-side and grid-side makes the rotor flux speed vary from sub-synchronous and super-synchronous speed. Both the photo-voltaic and wind generator need a maximum power point tracking (MPPT) control to allow maximum allowable power output. The distributed generators improve power system stability and enhance utility. The power electronic devices can sense the disturbances in the power system and triggers respective controls to mitigate disturbances [1] [2].

www.manaraa.com

CHAPTER 2: WIND GENERATOR

Wind turbine generators use a doubly-fed induction generator (DFIG) along with power electronic devices. The power converter converts between AC/DC based on power control and rotor frequency control. DFIG is variable speed induction generator. The sophisticated multi-loop control logic structure is a between the machine stator and the grid. DFIG system is subjected to undesirable dynamic interaction between grid and farm. Though there are some shortcomings, through simulation studies and design analysis, the system is concluded to be stable and robust.

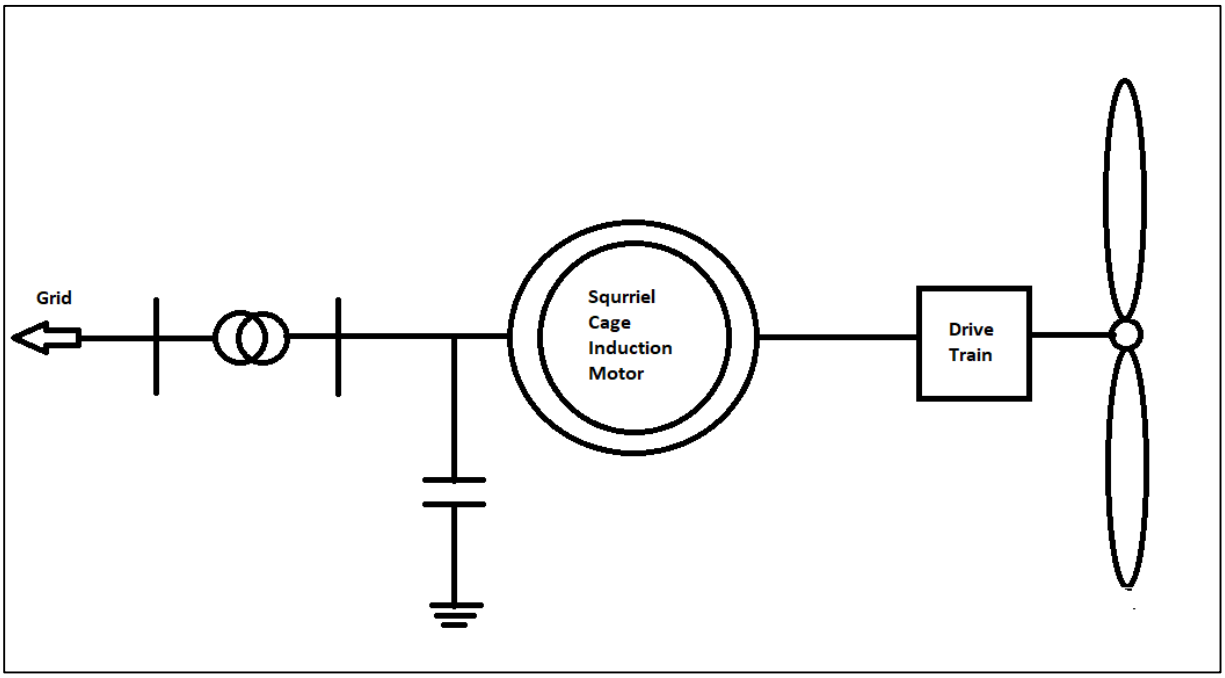

Figure 2.1 Type-1 Wind Turbine

There are four different types of wind turbines. Type-1 is a Squirrel Cage Induction generator connected directly to a transformer. As the turbine rotates at a speed faster than the synchronous speed, a negative slip will result. This will generate real power which will be injected

www.manaraa.com

into the grid. But one of the major disadvantages of the system is that, due to inertia, a sudden wind speed change will result in a limited change in electrical output.

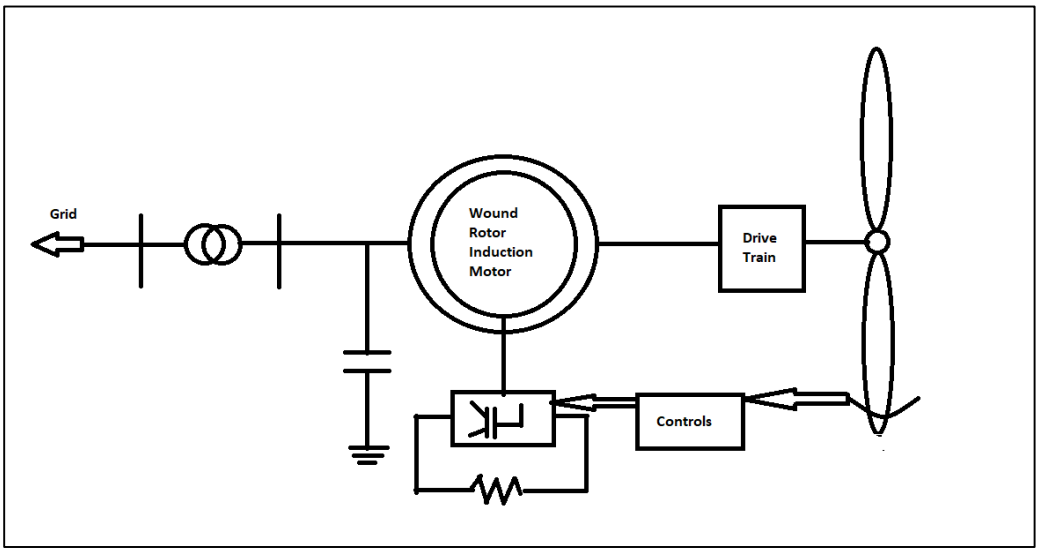

Figure 2.2 Type-2 Wind Turbine

In Type-2 the use of wound rotor is used. The connection is similar to Type-1, but an additional variable resistance is connected. This is done by adding a power electronic device and a rheostat to the rotor circuit. The current flows along the slip rings and the variable resistance. Adding resistances can control the flowing current into the rotor, but its drawback is, this could influence the dynamics of the system.

www.manaraa.com

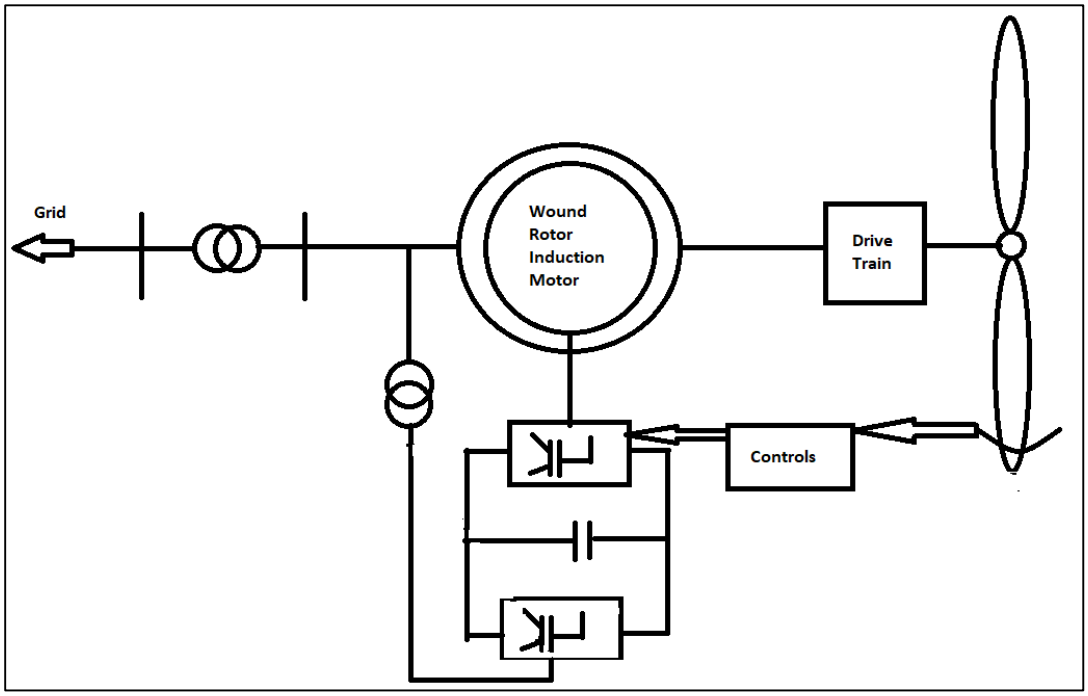

Figure 2.3 Type-3 Wind Turbine

Type-3 type wind turbines are called doubly-fed induction generator. The generator is fed by mechanical power and the rotor is fed with electrical power. At first, the power will be fed from the grid to the rotor. As the DFIG gets excited, it is going to provide power back to the grid from the stator. The dynamics behind the mechanical control is easy to implement and the regulation of output can be performed easily. The only disadvantage of this system is that, a capacitive component in series with the DFIG can lead to sub-synchronous resonance and which may damage the rotor and shaft system.

www.manaraa.com

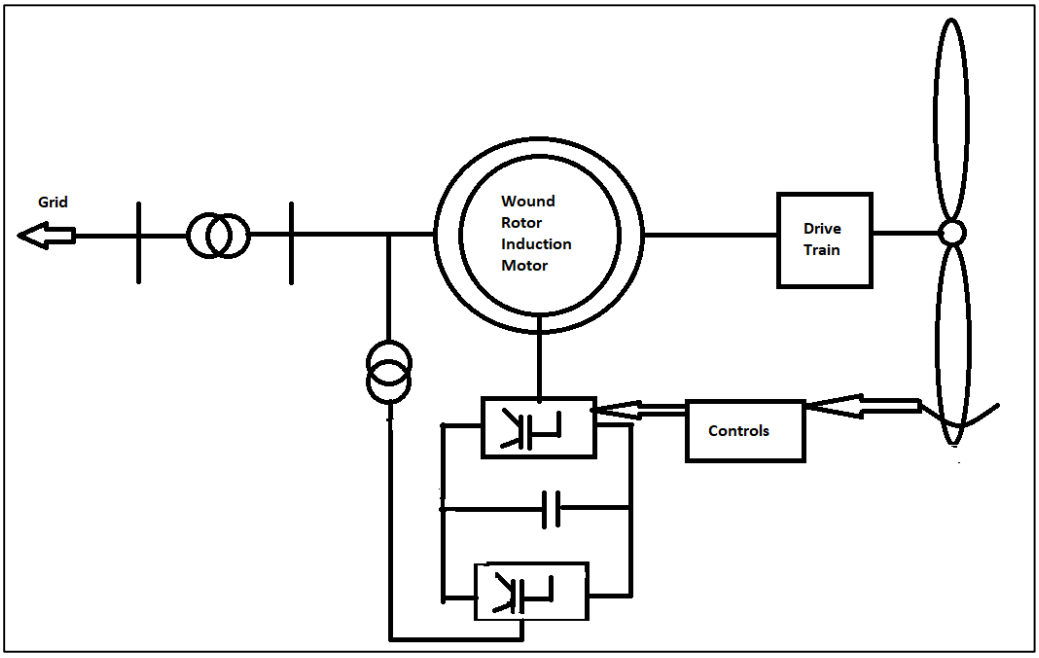

Figure 2.4 Type-4 Wind Turbine

The Type-4 wind turbine also called a full-converter wind turbine. This generator implements a permanent magnet in its rotor. This reduces rotor loss and it improves responses and faster decoupling. There is an AC-DC-AC converter which interfaces with the stator output and the grid. But this process is expensive to implement and research is going on to make it more efficient.

www.manaraa.com

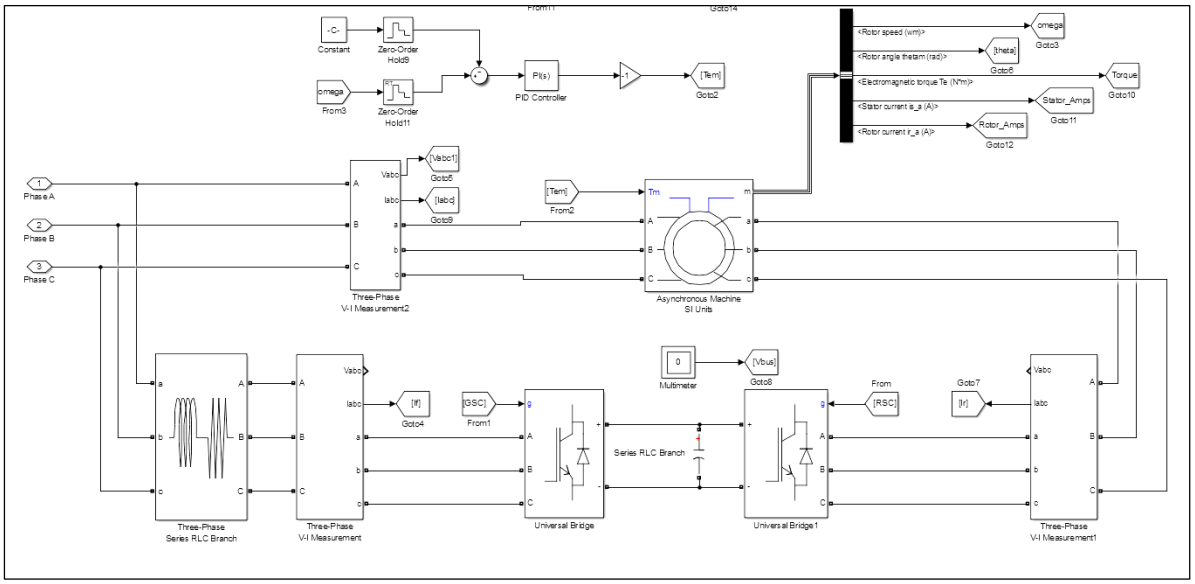

Figure 2.5 Simulation Model of Doubly Fed Induction Generator

In a state space model of DFIG, the electrical, electro-mechanical and mechanical systems are identified. The load in the alternator is inversely proportional to the rotor frequency. Hence, the increase of load in the alternator will result in a reduction of frequency, this will result in sub-synchronous frequency [3].

The scenario will result in resonance between the mass-spring system of the governor of the turbine and the series capacitor. Control loops in the grid-side converter (GSC) and rotor-side converter (RSC) are demonstrated in this paper. The MPPT control is used to maximize the power generation, it does so by calculating the reference torque for a given optimal power and rotor speed. The aim of the GSC and RSC is to control the steady-state of DFIG. The GSC controls the DC-link voltage and induction terminal voltage. The RSC controls the electric torque and stator reactive power [4] [5] [6].

2.1 Converter Control

- Vector Control controls the d-q frame rotor current aligned with the stator flux. In the q-frame electric torque is represented by rotor current and in d-frame rotor current is represented by the reactive power.

www.manaraa.com

- Direct Torque Control deals with the magnitude of rotor flux linkage and electric torque, to properly control the inverter on the rotor side. Using the stator and rotor current vectors, the machine flux is determined. The machine torque is determined using rotor current and rotor flux.
- Direct Power Control, unlike direct torque control, uses the rotor and stator flux to determine the real and reactive power. This is achieved by applying proper rotor voltage to the induction machine.

2.1.1 Grid-Side Converter (GSC) Control

The primary importance of GSC is to regulate the voltage at the DC-Link. It also allows real power to flow in the converter. Voltage Control and Direct Power Control is adopted to ensure independent real and reactive power control.

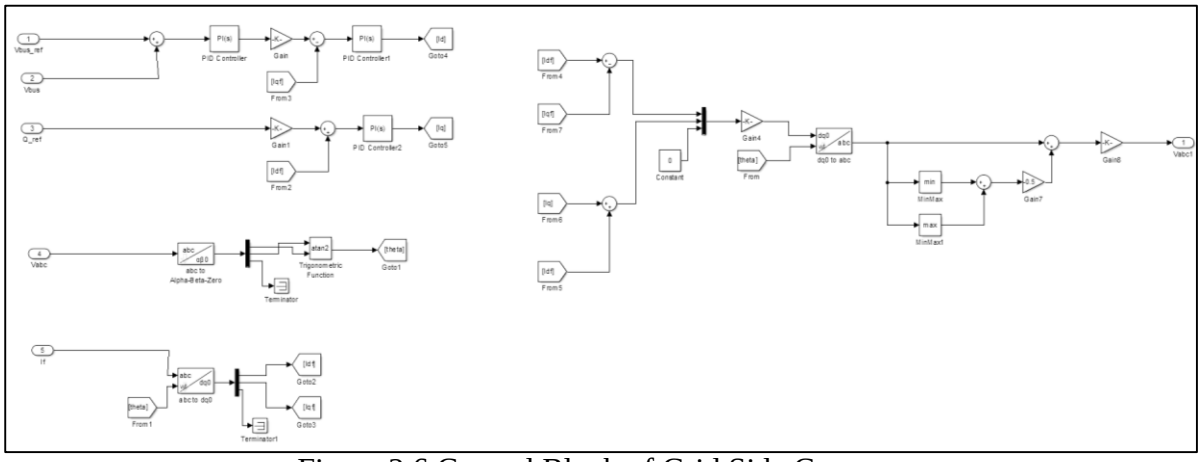

Figure 2.6 Control Block of Grid Side Converter

The input currents are the d-q frame currents of the grid and the d-q frame stator voltages. The grid current result from the algebraic sum of the respective d-q frame stator currents and line currents [7].

$$i_{qg} = i_{ql} + i_{qs} \quad (2.1)$$

$$i_{dg} = i_{dl} + i_{ds} \quad (2.2)$$

www.manaraa.com

On the other hand, the rotor voltages can be calculated using KVL (the algebraic sum of grid voltages and drop in the transformer) [7] [4] [1]:

$$v_{qs} = v_{qg} - i_{dg}X_{tg} \quad (2.3)$$

$$v_{ds} = v_{dg} + i_{qg}X_{tg} \quad (2.4)$$

2.1.1.1 Outer Loop Control

The reference value of V_{bus} is compared with the voltage across the DC link capacitor voltage. The difference is sent through a PI controller to evaluate the field [2].

$$i_{df}^{*} = k_{pf}\left(k_{pB} + \frac{k_{iB}}{s}\right)(V_{bus}^{*} - V_{bus}) \quad (2.5)$$

$$i_{qf}^{*} = k_{qf}Q^{*} \quad (2.6)$$

From the above equation, the value of proportionality constants is identified by using the trial and error method. The main motive was to improve the response time of the system. The values are chosen for $k_{pB} = -1000$ and for $k_{iB} = -300000$.

2.1.1.2 Inner Loop Control

The output from the PI controller becomes the reference current which is compared with the given current.

$$V_d = \left(k_{p_id} + \frac{k_{i_id}}{s}\right)\left(i_{df}^{*} - i_{df}\right) \quad (2.7)$$

$$V_q = \left(k_{p_iq} + \frac{k_{i_iq}}{s}\right)\left(i_{qf}^{*} - i_{qf}\right) \quad (2.8)$$

In the above equation, we have defined the PI controller parameters. The PI controller has got two parts, a proportional controller (k_p) and an integrator controller (k_i).

www.manaraa.com

$$k_{p_id} = (2\omega_{ni}\sigma L_r) - R_r \quad (2.9)$$

$$K_{i_id} = \omega_{ni}^2 L_r \sigma \quad (2.10)$$

From equation (2.9) and (2.10), L_r is called the rotor inductance. The other unknowns are defined as:

$$\omega_{ni} = \frac{100}{\tau_i} \quad (2.11)$$

$$\sigma = 1 - \frac{L_m^2}{L_s L_r} \quad (2.12)$$

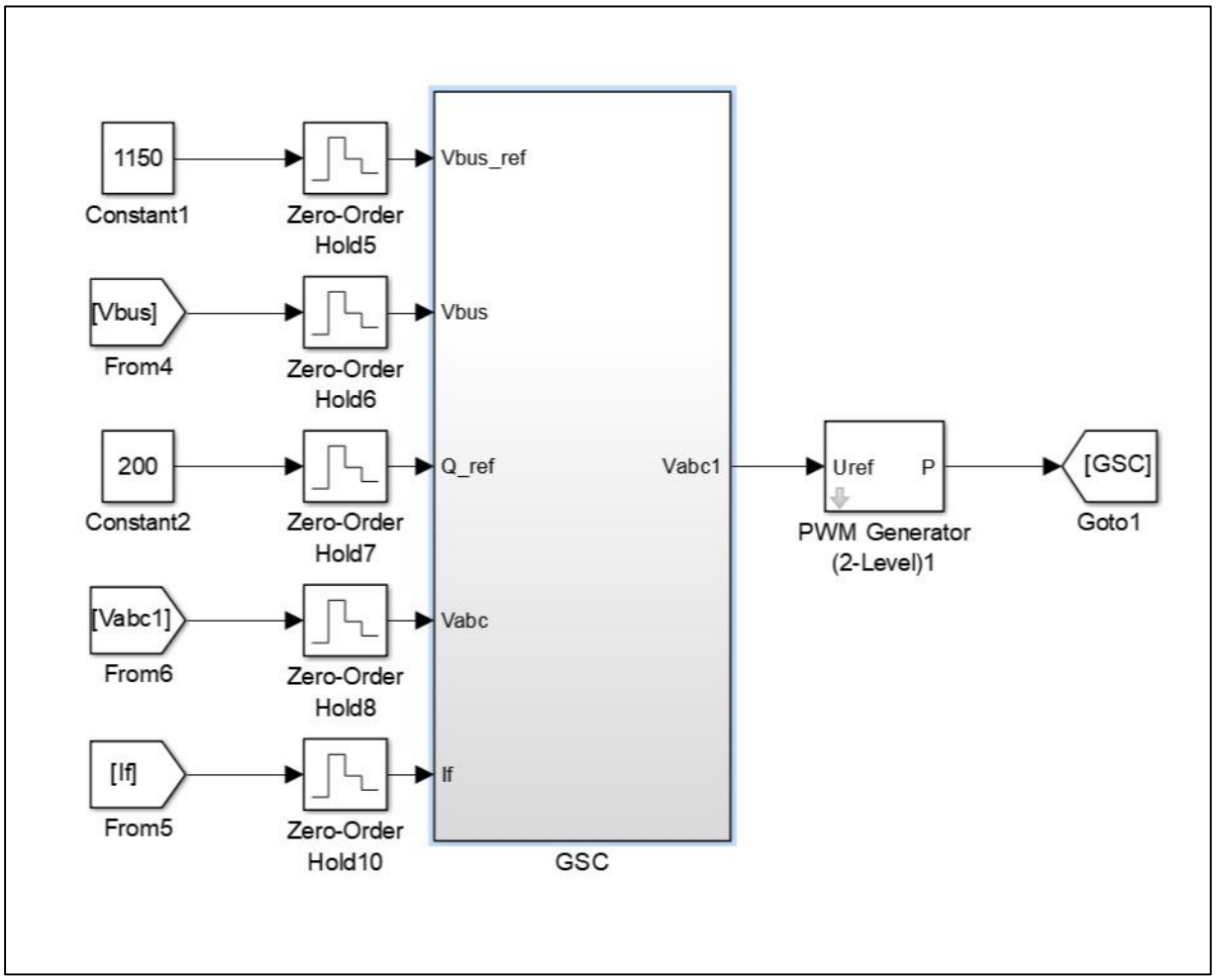

Figure 2.7 Subsystem Block of Grid Side Converter

www.manaraa.com

2.1.2 Rotor-Side Converter (RSC) Control

The primary objective is to control of electric torque and the power factor of stator terminals is done by the RSC. The control strategies include vector control, direct torque control, and direct power control. The reactive power stored is given by:

$$Q_s = 0.5\left(v_{qs} i_{ds} - v_{ds} i_{qs}\right) \quad (2.13)$$

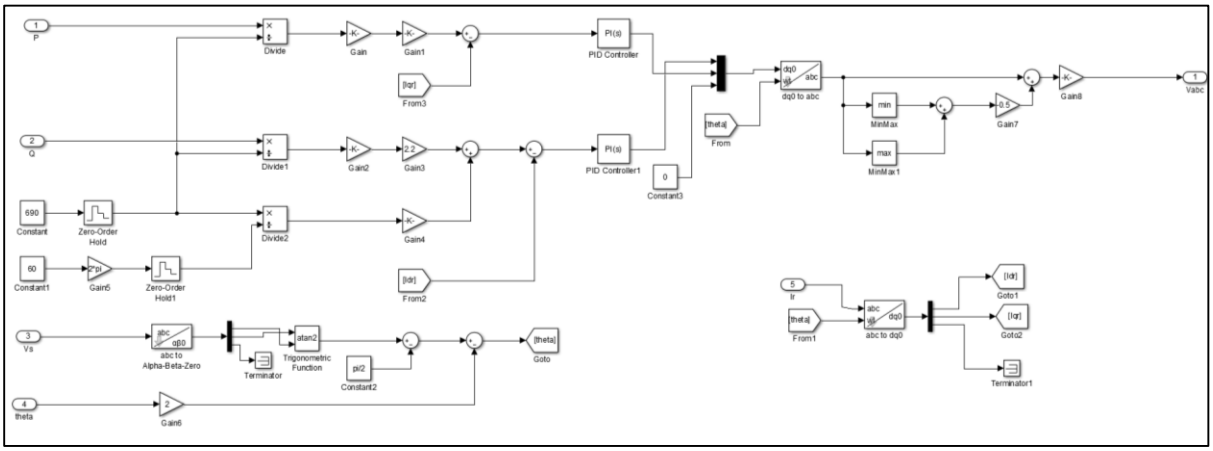

Figure 2.8 Control Block Diagram of Rotor Side Converter

2.1.2.1 Outer Loop Control

The reference value of Vbus is compared with the voltage across the DC link capacitor voltage. The difference is sent through a PI controller to evaluate the field.

$$i_{dr}^{*} = \left(\frac{-2L_s}{3L_m} k_d \frac{P}{V}\right) - \left(\frac{V_s}{\omega_s L_m}\right) \quad (2.14)$$

$$i_{qr}^{*} = \left(\frac{-2L_s}{3L_m} k_q \frac{Q}{V}\right) \quad (2.15)$$

2.1.2.2 Inner Loop Control

The reference value of currents is taken here in the respective d-q frame. The difference is sent through a PI controller to evaluate the field.

$$V_d = \left(k_{p_idf} + \frac{k_{i_idf}}{s}\right)\left(i_{df}^{*} - i_{df}\right) \quad (2.16)$$

www.manaraa.com

$$V_q = 100\left(k_{p_{iq}} + \frac{k_{i_{iq}}}{s}\right)\left(i_{qf}^{*} - i_{qf}\right) \quad (2.17)$$

The above equation has been represented by proportionality and integration constants. They are defined by:

$$k_{p_idf} = \left(2\omega_{nig}L_g\right) - R_g \quad (2.18)$$

$$k_{i_idf} = \omega_{nig}^2 L_g \quad (2.19)$$

$$\omega_{nig} = 2\pi 60 \quad (2.20)$$

$$k_{pf} = \frac{1}{1.5V_s\frac{\sqrt{2}}{\sqrt{3}}} \quad (2.21)$$

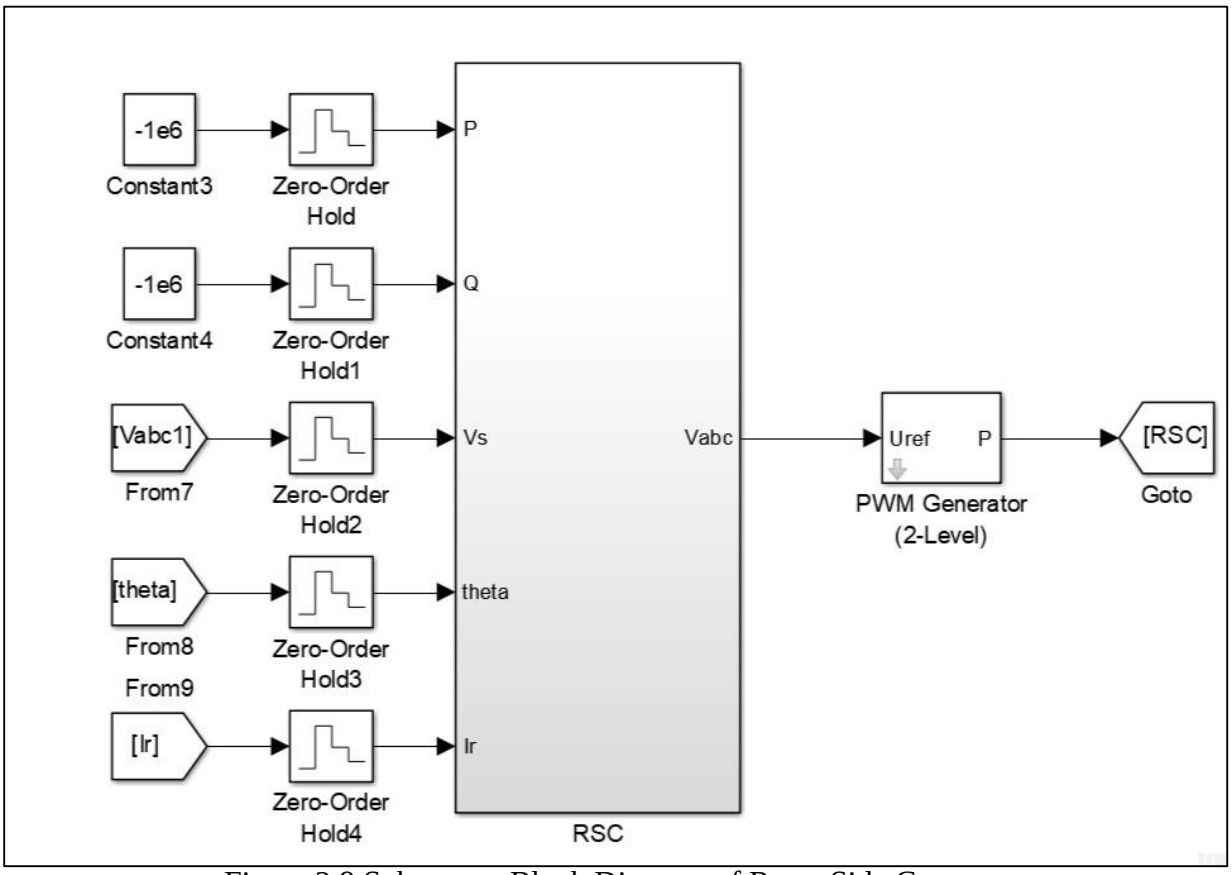

Figure 2.9 Subsystem Block Diagram of Rotor Side Converter

www.manaraa.com

2.1.3 DC-Link

The DC-Link is the common portion between the DFIG and the grid. The capacitor dynamics is related to the stator and rotor active power [8].

$$-CV_{DC}\frac{dV_{DC}}{dt} = P_r + P_g \quad (2.22)$$

where P_r and P_g are given by:

$$P_r = 0.5\left(v_{dr}i_{dr} + v_{qr}i_{qr}\right) \quad (2.23)$$

$$P_g = 0.5\left(v_{dg}i_{dg} + v_{qg}i_{qg}\right) \quad (2.24)$$

2.2 Wind Turbine

The wind generator converts wind power to mechanical power. The reference angular speed is compared to the machine's angular speed and the difference is passed through a PI controller to generate torque of the to the machine. The following equations explain the functionality:

$$T_{em} = -(K_{pv} + \frac{K_{iv}}{s})(\omega^* - \omega) \quad (2.25)$$

$$k_{p_v} = \frac{2\omega_{nn}J}{p} \quad (2.26)$$

$$k_{i_v} = \frac{\omega_{nn}^2 J}{p} \quad (2.27)$$

2.3 Doubly-fed Induction Generator

The induction generator is a system of differential equations in state space system. Using abc-dq transformation, the system is represented in a synchronously rotating frame. The state space equation is given by [3]:

$$\dot{X}_{DFIG} = A_{DFIG}X_{DFIG} + B_{DFIG}U_{DFIG} \quad (2.28)$$

www.manaraa.com

$$X_{DFIG} = [i_{qs} \quad i_{ds} \quad i_{0s} \quad i_{qr} \quad i_{dr} \quad i_{0r}]^T \quad (2.29)$$

$$U_{DFIG} = [v_{qs} \quad v_{ds} \quad v_{0s} \quad v_{qr} \quad v_{dr} \quad v_{0r}]^T \quad (2.30)$$

The values of A_{DFIG} and B_{DFIG} are calculated by the set of matrix equations.

$$F = \begin{pmatrix} R_s & \frac{\omega_e}{\omega_b}X_{ss} & 0 & 0 & \frac{\omega_e}{\omega_b}X_m & 0 \\ \frac{\omega_e}{\omega_b}X_{ss} & R_s & 0 & \frac{\omega_e}{\omega_b}X_m & 0 & 0 \\ 0 & 0 & R_s & 0 & 0 & 0 \\ 0 & \frac{\omega_e-\omega_r}{\omega_b}X_m & 0 & R_r & 0 & \frac{\omega_e-\omega_r}{\omega_b}X_m \\ -\frac{\omega_e-\omega_r}{\omega_b}X_m & 0 & 0 & \frac{\omega_e-\omega_r}{\omega_b}X_{rr} & R_r & 0 \\ 0 & 0 & 0 & 0 & 0 & R_r \end{pmatrix} \quad (2.31)$$

$$G = \begin{pmatrix} X_{ss} & 0 & 0 & X_m & 0 & 0 \\ 0 & X_{ss} & 0 & 0 & X_m & 0 \\ 0 & 0 & X_{ls} & 0 & 0 & 0 \\ X_m & 0 & 0 & X_{rr} & 0 & 0 \\ 0 & X_m & 0 & 0 & X_{rr} & 0 \\ 0 & 0 & 0 & 0 & 0 & X_{lr} \end{pmatrix} \quad (2.32)$$

$$A_{DFIG} = -\omega_b G^{-1} F \quad (2.33)$$

$$B_{DFIG} = -\omega_b G^{-1} \quad (2.34)$$

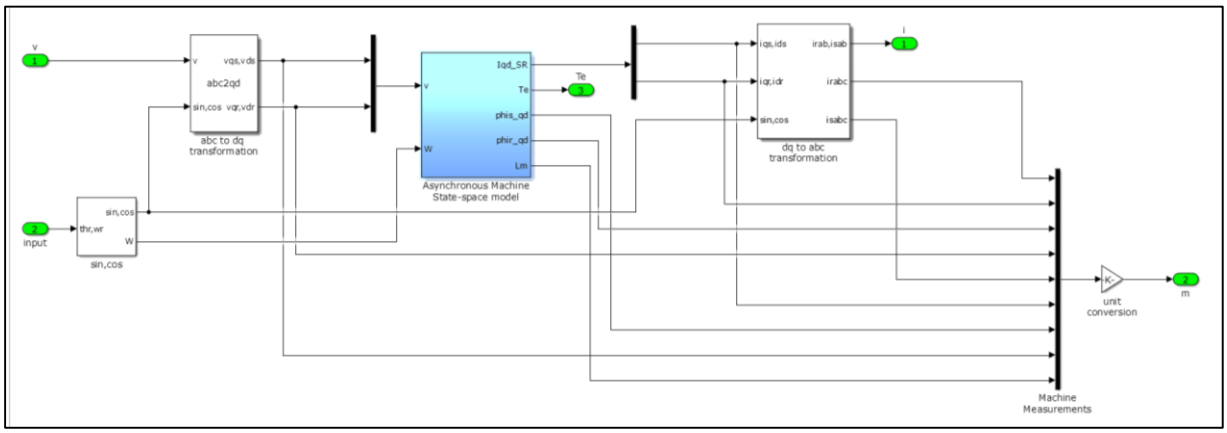

Figure 2.10 State Space Model of Doubly Fed Induction Generator

www.manaraa.com

2.4 Shaft System

This system is treated as the two-mass system. They are the low-speed turbine and the high-speed turbine. In order to connect to connect the two-mass system, the spring damper technique is used. The system of differential equations to guide the operation is given by:

$$\dot{X}_{SHAFT} = A_{SHAFT}X_{SHAFT} + B_{SHAFT}U_{SHAFT} \quad (2.35)$$

From the above equation, we can define the variables in the following equations as:

$$X_{SHAFT} = [\bar{\omega}_m \quad \bar{\omega}_r \quad T_{tg}]^T \quad (2.36)$$

$$U_{SHAFT} = [\bar{T}_\omega \quad T_e \quad 0]^T \quad (2.37)$$

$$A_{shaft} = \begin{pmatrix} \frac{-D_t - D_{tg}}{2H_t} & \frac{D_{tg}}{2H_t} & \frac{-1}{2H_t} \\ \frac{D_{tg}}{2H_g} & \frac{-D_t - D_{tg}}{2H_g} & \frac{-1}{2H_g} \\ K_{tg}\omega_b & -K_{tg}\omega_b & 0 \end{pmatrix} \quad (2.38)$$

$$B_{shaft} = \begin{pmatrix} \frac{1}{2H_t} & 0 & 0 \\ 0 & \frac{1}{2H_g} & 0 \\ 0 & 0 & 1 \end{pmatrix} \quad (2.39)$$

From the above equations, $\bar{\omega}_m$ is the turbine shaft. $\bar{\omega}_r$ is the generator speed. $\bar{T}_\omega$ is the wind torque. D_g and D_t are damping coefficients of generator and turbine. H_g and H_t are the inertia constants of the generator and turbine coefficients. Using the MPPT control the optimal value of the wind torque is calculated. It is given by:

$$\psi_{qm} = X_m(i_{qs} + i_{qr}) \quad (2.40)$$

$$\psi_{dm} = X_m(i_{ds} + i_{dr}) \quad (2.41)$$

$$T_e = 0.5(\psi_{qm}i_{dr} - \psi_{dm}i_{qr}) \quad (2.42)$$

www.manaraa.com

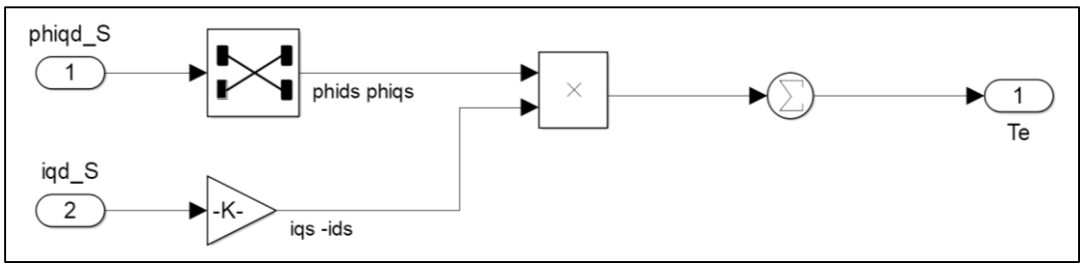

Figure 2.11 Simulation Model of Torque Calculations

www.manaraa.com

CHAPTER 3: PHOTOVOLTAIC CELL

3.1 Basics of Photovoltaic (PV) Cell

PV cells are made up of single crystalline or polycrystalline silicon. The efficiency ranges from 11-15%. They are expensive in cost due to thickness. But with the recent development of thin film material like copper indium selenide and cadmium telluride, the cost was greatly reduced with considerable efficiency [9].

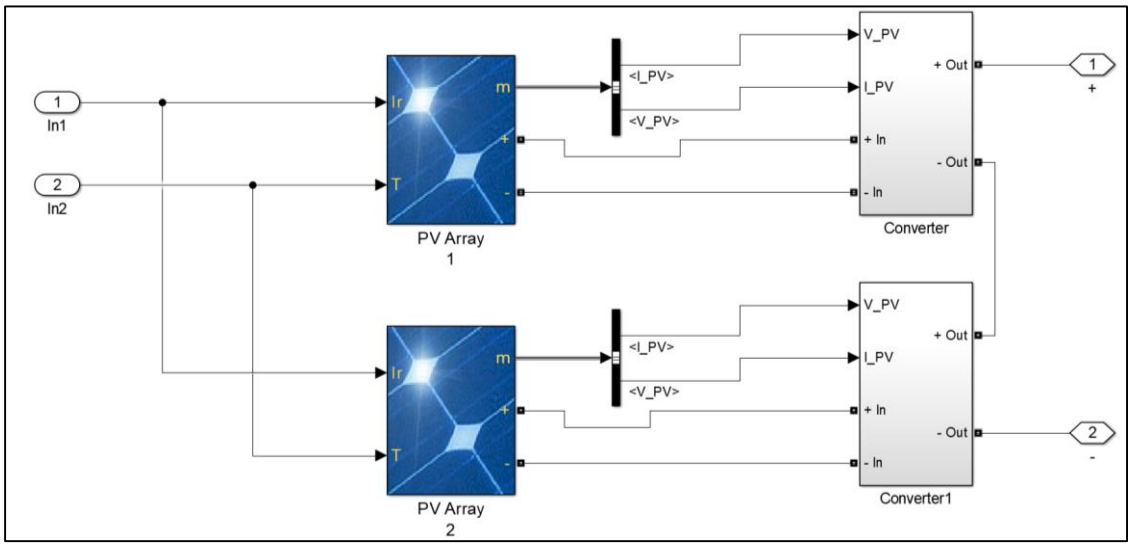

Figure 3.1 Simulation Model of Photovoltaic System

The equivalent circuit of a PV Cell is given by a diode connected in parallel with a current source. The output current of a PV cell is given by:

$$I_{PV} = I_{SC} - I_S\left(e^{\frac{V_D}{\eta V_T}} - 1\right) - \frac{V_D}{R_P} \quad (3.1)$$

From the above equation V_T is considered to be thermal voltage and the value is 26mV at room temperature. η is called the efficient coefficient, values from 1 to 2. The parallel resistances

www.manaraa.com

is given by R_p and the series resistances R_s. External factors like temperature, shading and bypass diode configuration [10].

3.2 Step-Up Converter

Step-Up converters, also known as boost converters, converts low voltage DC input to high voltage DC output. An IGBT switch controls the level of voltage. The duty cycle of the converter is defined by the amount of time the switch is turned ON. The voltage boost is given by:

$$\frac{V_o}{V_d} = D\frac{1}{1-D} \quad (3.2)$$

From the above equation, the output voltage is given by V_o the input voltage is given by V_d and D represents the duty ratio. The boost converter steps-up the output from the PV cell and sent it to the converter before reaching the three phase converter. The input of the converter faces an inductor which stores the charge in the first cycle. At this stage, the switch is turned OFF. When the switch is turned ON, the input current as well as the inductor current passes through, hence there is a boost of energy.

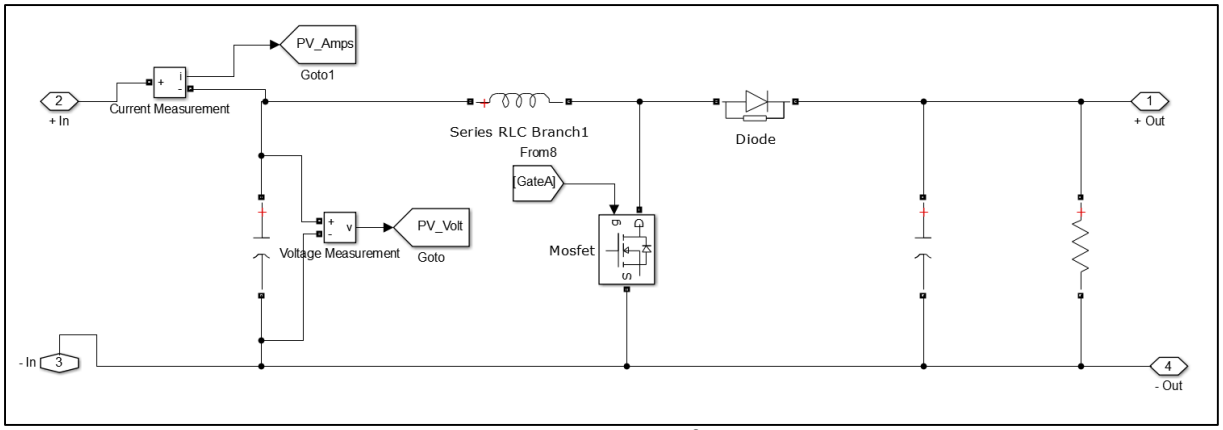

Figure 3.2 Simulation Model of Step-Up Converter

www.manaraa.com

3.3 Maximum Power Point Tracking

The PV cell works at a certain point in the current-voltage curve. This point is called the operating point. Now we know that power is voltage times current. The operating point on the current-voltage curve will correspond to an operating point on the power-voltage curve. So it is always wise to operate at the maximum peak of power on the power-voltage curve. This point is called maximum power point and it corresponds to the peak of the power-voltage curve. This point is fixed only if ambient conditions like irradiance and temperature, are kept constant. A change in any of the criteria will produce a different current-voltage and power-voltage cure. Now we have to figure out the new power point and this process is called the maximum power point tracking. MPPT tracking can be classified as follows:

- Indirect Method
    - Fixed Voltage Method
    - Fractional Open Circuit Method
- Direct Method
    - Perturb and Observe Method
    - Incremental Conductance Method

3.3.1 Fixed Voltage Method

This method makes simple assumptions to estimate MPPT periodically. The measurement methods are very simple. This method adjusts the operating voltage level on a seasonal basis. Higher maximum power point is expected in winter and lower maximum power point in summer, for the same value of irradiance. This method is not very accurate, as the irradiance is assumed to be constant.

www.manaraa.com

3.3.2 Fractional Open Circuit Method

This is a very common indirect method which tracks the maximum power point. This technique exploits the fact that a good approximation of the maximum power point voltage is some function of the open circuit voltage. So maximum power point voltage is some constant times open circuit voltage. The constant can be determined by the type of silicon and how the PV cell is used. For a different value of irradiance, the current-voltage curve changes, but the ratio of maximum power point to open circuit voltage, shows little change. This method is very easy to implement, as the technique is very straight forward. But on the flip side, the process of approximation does not always give the correct operating point. Every time there is a change in irradiance condition, the open circuit voltage has to be measured. This is done by temporarily disconnecting the system from its load. This results in a temporary loss of power.

3.3.3 Perturb and Observe Method

This is a more evolved technique of maximum power point tracking. This provides an accurate and faster response because it measures the current, voltage and power directly. If the increase in voltage results in increase in power, it means the maximum power point is on the left side of the operating point. Hence further voltage boosting is needed to reach the maximum power point. If the increase in voltage results in decrease in power, then the operating point is on the right-hand side of maximum power point and hence voltage has to be reduced in order to reach the maximum power point. This method uses the advantage of the current-voltage curve. It is increasing in nature towards the left and decreasing in nature towards the right of the power point. The only disadvantage is that the operating point is never fixed and is always hovering on the maximum power point region and hence several perturb and observe algorithm needs to be executed [11].

www.manaraa.com

Severe changes in weather conditions can lead to a detrimental effect on the convergence system. Change in illumination can create a different power-voltage curve and hence the maximum power point may shift, so the algorithm has to adjust accordingly to meet the requirements.

3.3.4 Incremental Conductance Method

Electrical conductance is given by the ratio of current to voltage. The slope of the current-voltage curve gives conductance. The slope is zero at maximum power point, hence there is no conductance. So now we have,

$$\frac{dP}{dV} = \frac{d(I.V)}{dV} = I + V.\frac{dI}{dV} \quad (3.3)$$

Since the sampling time is less, we can approximate $\frac{dI}{dV}$ as $\frac{\Delta I}{\Delta V}$. So the following conclusions are drawn:

$$\frac{\Delta I}{\Delta V} = -\frac{I}{V} \; at\ maximum\ power\ point$$

$$\frac{\Delta I}{\Delta V} > -\frac{I}{V} \; left\ of\ maximum\ power\ point$$

$$\frac{\Delta I}{\Delta V} < -\frac{I}{V} \; right\ of\ maximum\ power\ point$$

This method measures between the instantaneous conductance and change in conductance and it decides whether the operating point is to the left or right of the maximum power point. The drawback of this method is that, in very high changing conditions, this method can be a problem, due to small sampling intervals. It is difficult to implement as it will have to measure the instantaneous and incremental conductance every time.

www.manaraa.com

The maximum power point tracking (MPPT) takes the output from the PV cell and compares with the reference signals. The error signal is sent to the PI controller, and the duty cycle is obtained. This duty cycle is the gate signal for the DC-DC converter.

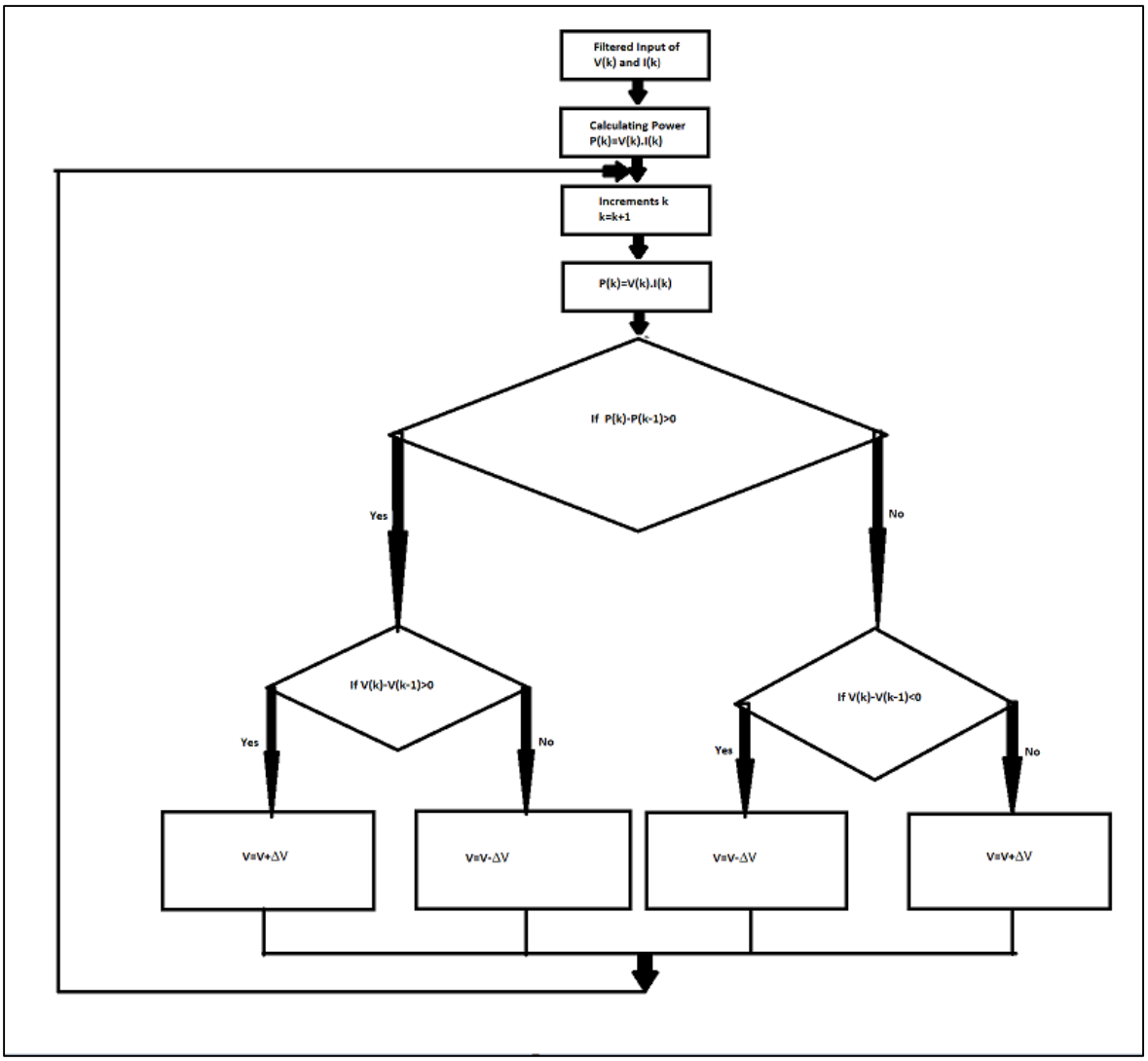

Figure 3.3 Algorithm of Maximum Power Point Tracking

The MPPT method adopts the perturb and observe method. The control of the voltage is done by the measure of power in the PV array. If the power increases, the voltage is adjusted, so that there is no more increase in power.

www.manaraa.com

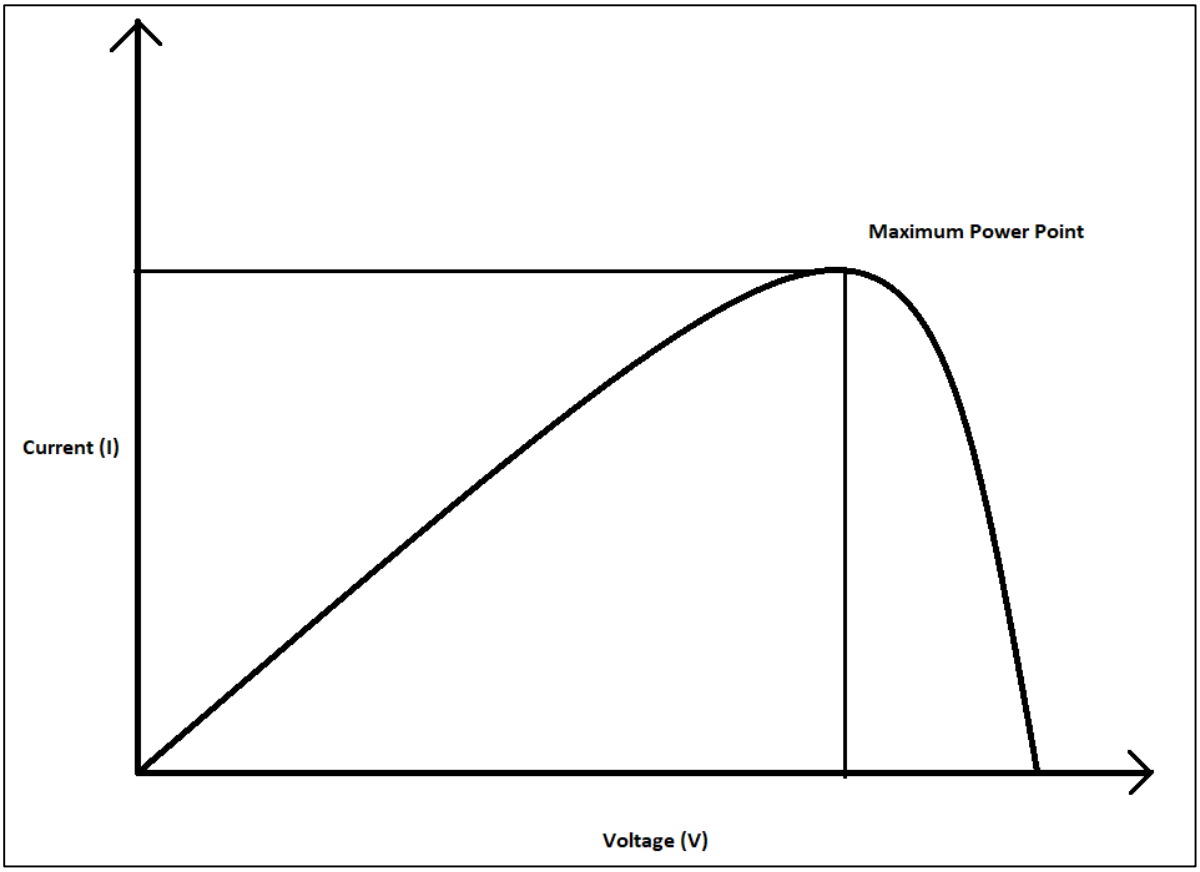

Figure 3.4 Graph of Maximum Power Point Tracking

This method is called the hill climbing method. This is dependent on the rise of the curve of power against voltage, below the operating point. This method is the most popular method and eases to implement. This method results in top-level efficiency, with proper predictive analysis and adoptive hill climbing strategy.

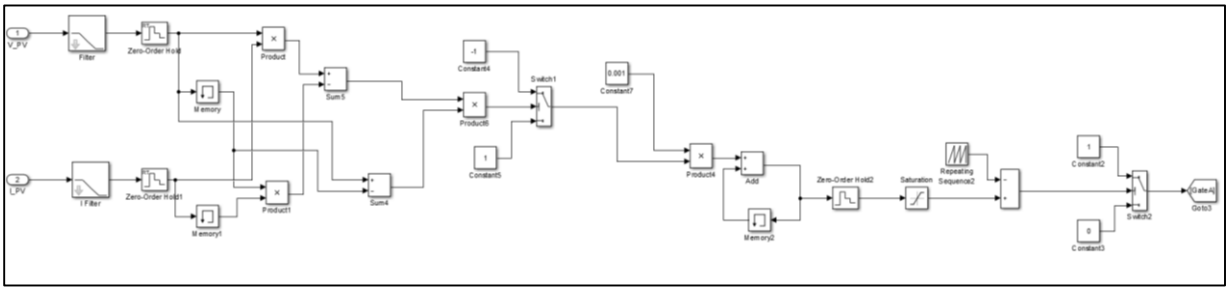

Figure 3.5 Simulation Model of Maximum Power Point Tracking

www.manaraa.com

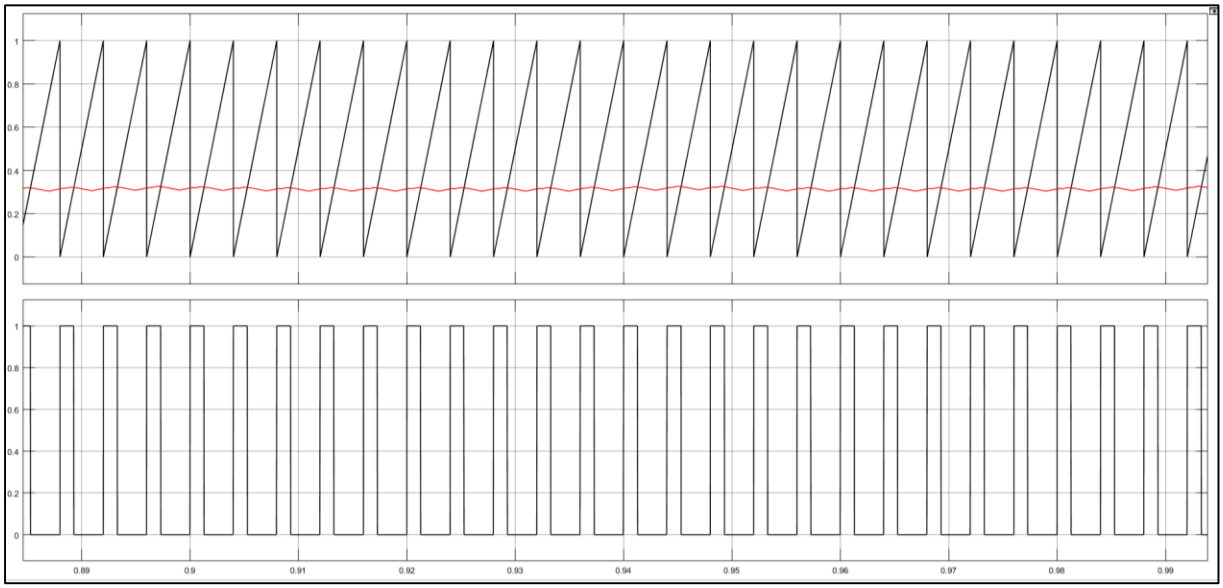

Figure 3.6 Switching Pulse

www.manaraa.com

CHAPTER 4: FUEL CELL

4.1 Introduction to Fuel Cell

The fuel cell contains two electrodes: anode and cathode. The fuel is brought in through the pipe and is channeled to the anode. While on the cathode side, fresh air is channeled in. Hydrogen breaks into its ionic form $2H^+$ form, thus releasing two negatively charged electrons $2e^-$. These electrons pass through the circuit as electric currents, while the hydrogen ion oxidizes to form water on the cathode side [12].

4.2 Power Electronics Circuit for Fuel Cell

4.2.1 Control Logic

In order to perform a power conditioning system, the fuel cell is connected to a DC-DC converter and the gate signal is converted by a closed loop control. The reference voltage is compared with the given voltage and the error signal is passed through a comparator. The output of the comparator is compared with the sawtooth waveform and the gate signal is generated for the DC-DC converter [11].

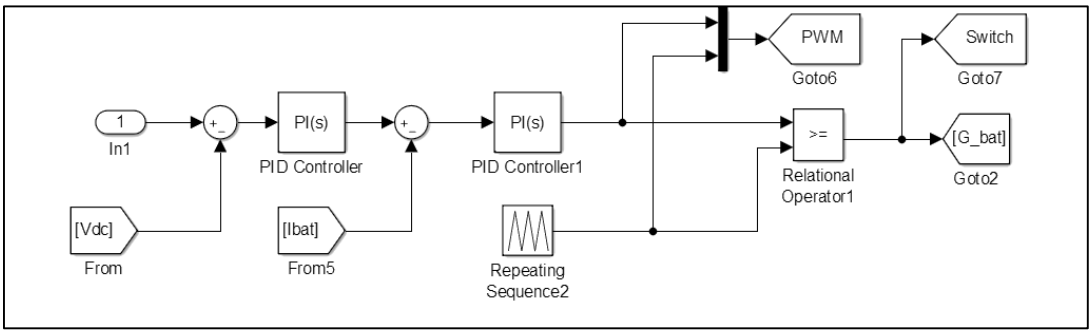

Figure 4.1 Simulation Model of Control Block

www.manaraa.com

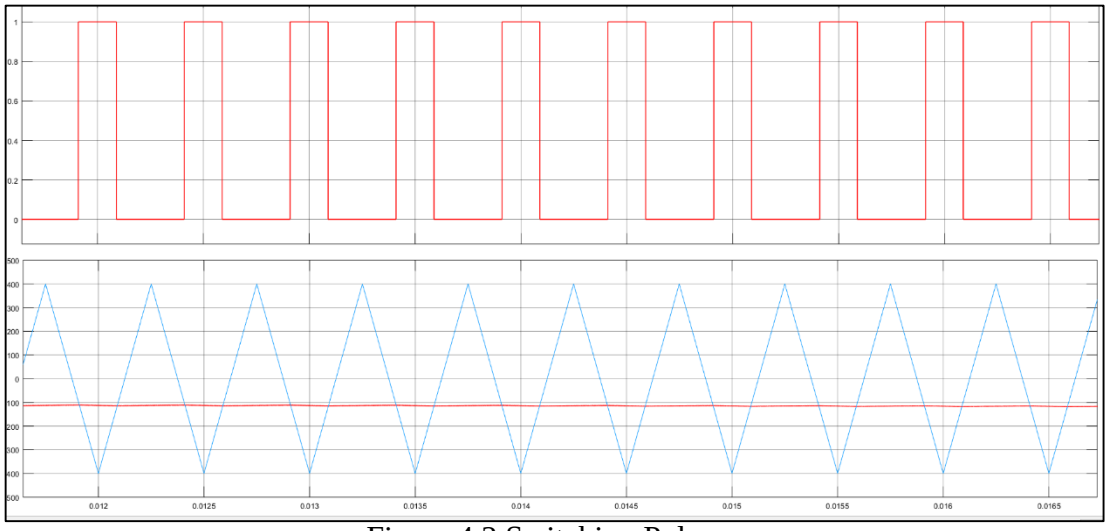

Figure 4.2 Switching Pulse

4.2.2 DC-DC Converter

The voltage converter is used to step up the battery voltage. As the gate signal turns on the circuit, the boosted voltage is sent to the DC link along with the PV cell output. The main aim is to maintain a constant voltage in the DC-link so that even though the PV-cell fails to provide power, the battery will cover up and the system will stay running [13].

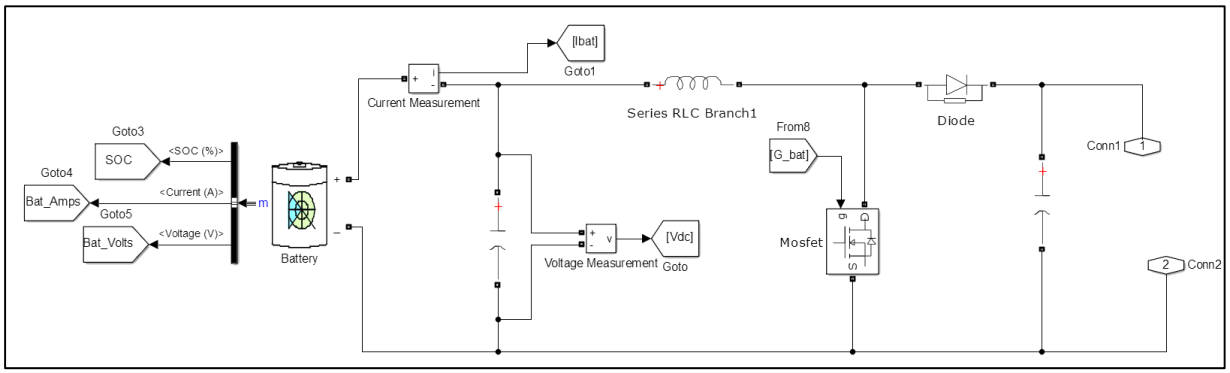

Figure 4.3 Simulation Model of Fuel Cell Circuit

www.manaraa.com

CHAPTER 5: THREE-PHASE INVERTER

5.1 Introduction

Switch mode DC to AC converters are called inverters. They are widely used in ac motor drives and uninterrupted ac power supplies. Switch-mode inverters can work both ways. If the switch is turned on then power flows from DC to the AC side. But if the diodes are left alone, they can function as a three-phase rectifier, converting three-phase AC power to DC power. In this paper pulse width modulation (PWM) inverter is used. In this type, the DC input is fairly constant. The inverter takes care of the magnitude and the frequency. Using PWM switches the AC output can be shaped as sinusoidal as possible [14].

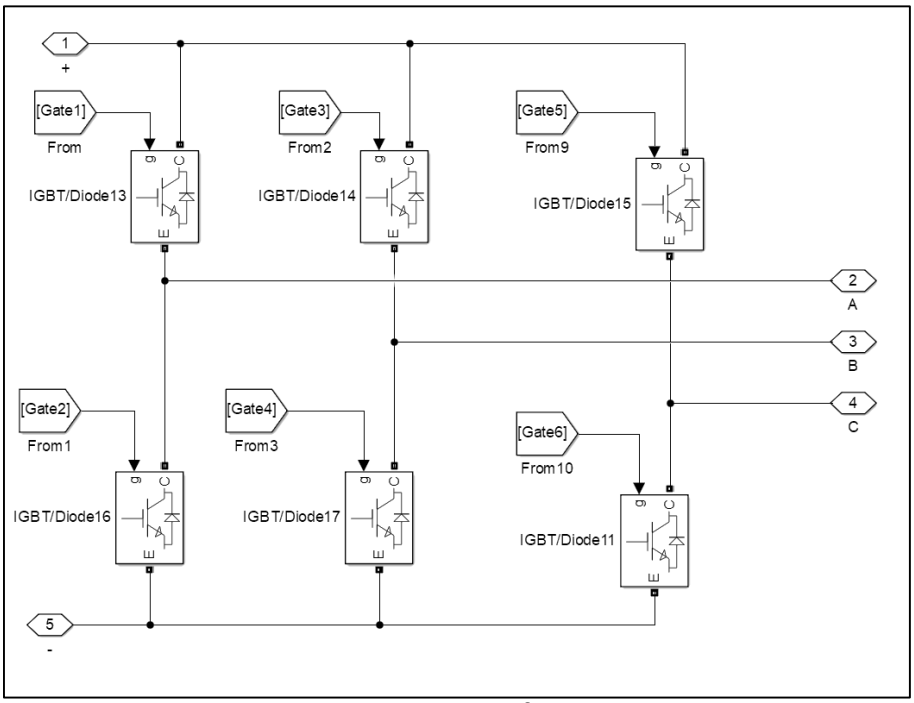

Figure 5.1 Simulation Model of Three-Phase Inverter

www.manaraa.com

5.2 Pulse Width Modulation Switching Scheme

This paper throws light on the sinusoidal PWM switching scheme. In this scheme, sinusoidal signals compared with a saw-tooth waveform. In order to create a sinusoidal output, three sinusoidal waves created, with 120^o out of phase and these waves are compared with the saw-tooth voltage. In linear modulation, the fundamental frequency is the frequency of the output voltage. The peak line-to-neutral voltage is given by:

$$\hat{V}_{AN} = m_a \frac{V_d}{2} \quad (5.1)$$

The amplitude modulation is given by m_a (≤ 1 for linear modulation) and the dc input voltage is given by V_d.

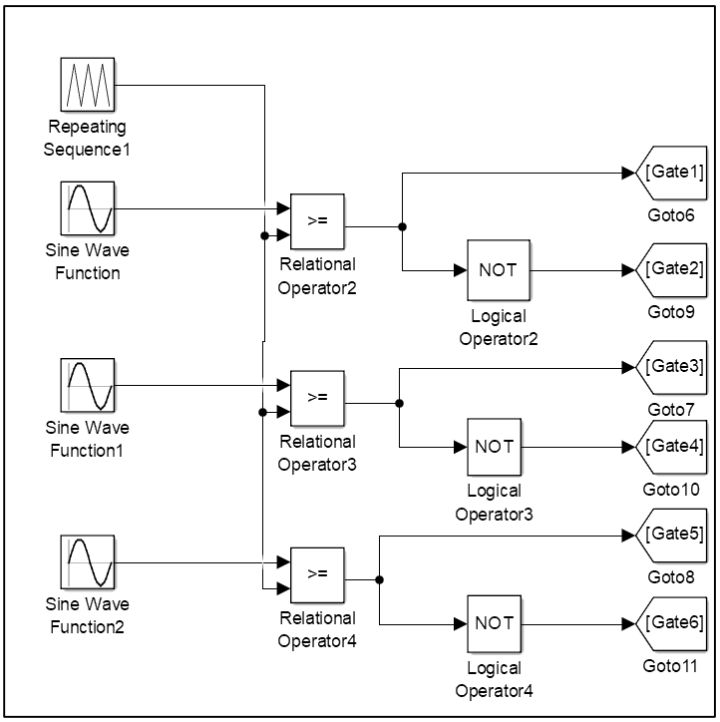

Figure 5.2 Simulation Model of Sinusoidal PWM

www.manaraa.com

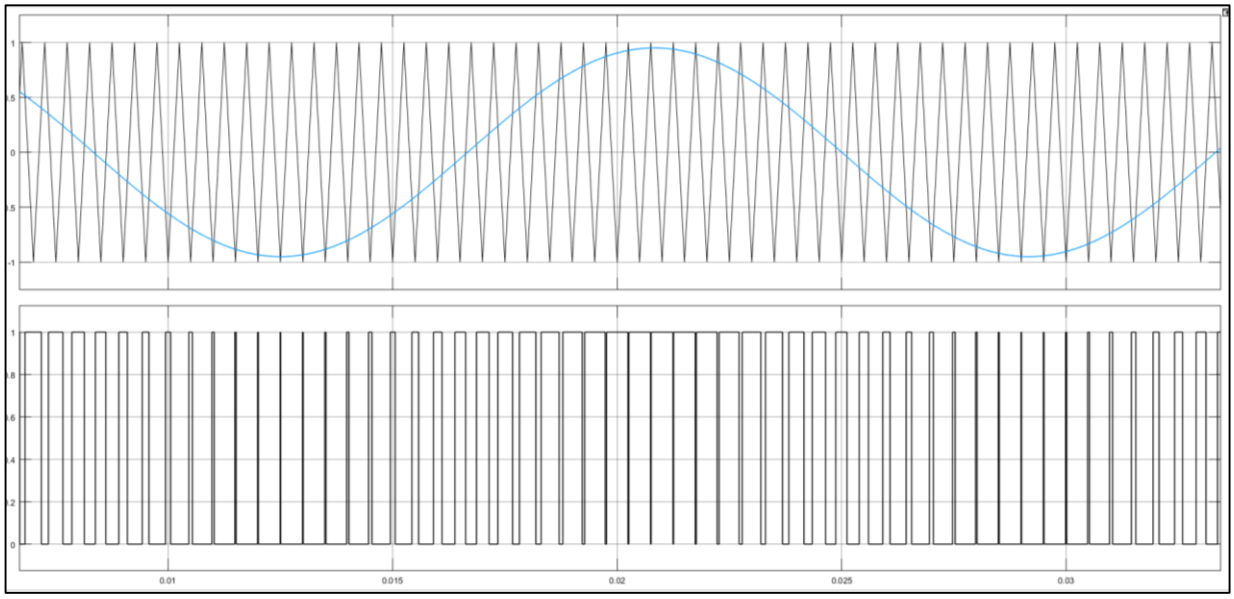

Figure 5.3 Graph of Sinusoidal PWM

www.manaraa.com

CHAPTER 6: ZERO ORDER HOLD

The zero order hold (ZOH) is a signal constructing a mathematical model which converts the analog and digital signal. Its MATLAB block can be found in the simulation library.

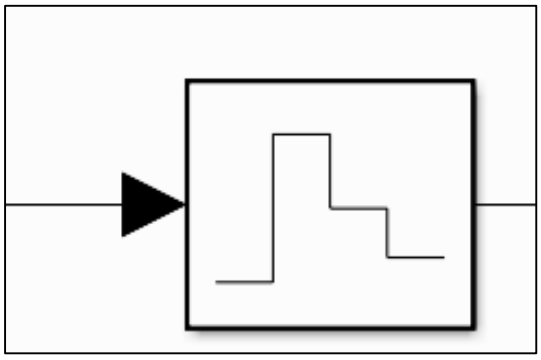

Figure 6.1 Zero Order Hold Block

This function converts discrete-time signal to the continuous-time signal. This is done by holding a sample signal over a period of time. ZOH is an important component in electrical system communications.

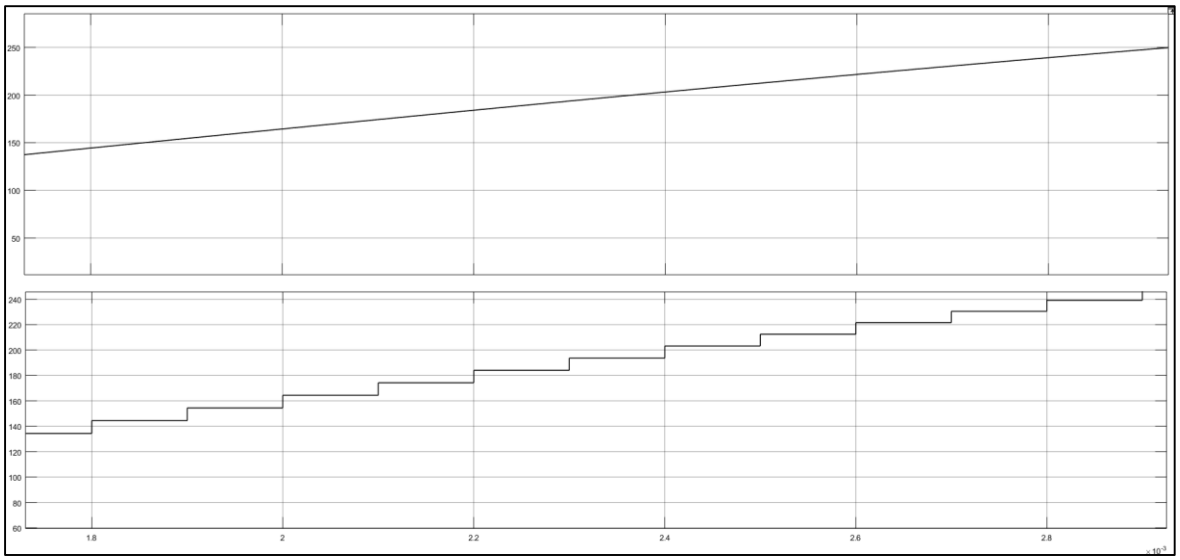

Figure 6.2 Zero Order Hold Graph

www.manaraa.com

The mathematical expression can be expressed with time-domain and in frequency domain analysis.

In the time domain, the waveform is reconstructed as sampling time T, from the $x[n]$ sequence of data and is given by:

$$x_{ZOH}(t) = \sum_{n=-\infty}^{\infty} x[n].rect\left(\frac{t - \frac{T}{2} - nT}{T}\right) \quad (6.1)$$

From the above equation, rect() is a rectangular function and $x_{ZOH}(t)$ is a piece-wise linear function. In frequency domain, the equation looks like this

$$x_{ZOH}(t) = \sum_{n=-\infty}^{\infty} x[n].\sigma\left(\frac{t - \frac{T}{2} - nT}{T}\right) \quad (6.2)$$

Zero-Order Hold block holds the input for a specific time and samples it. The time between the samples can be specified. The sample rate transforms between fast and slow response. The Zero-Order Hold block transforms fast to slow response. In order to receive the opposite, we can use a unit delay.

www.manaraa.com

CHAPTER 7: MATLAB BLOCKS

This project uses several MATLAB blocks to simulate the result. These blocks have indeed their own importance. They are obtained from various simulation libraries. They are listed as follows:

7.1 Memory

This block delays the input by one integration time. When it placed with an integration system, it holds and delays the input by one step and it can accept both discrete and continuous signals. If the input is a vector, then the output gets delayed by a vector step. This block is a single input single output system. The block asks for initial parameters for the first step time.

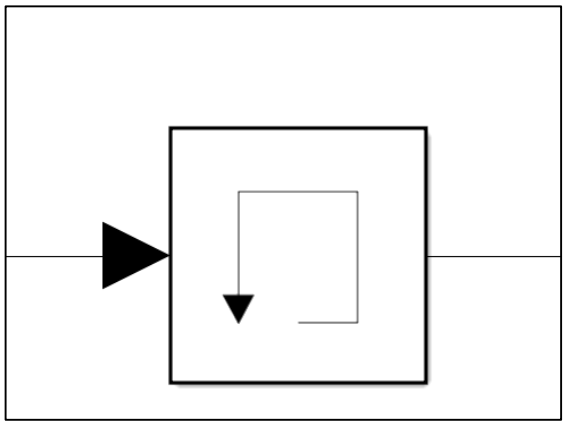

Figure 7.1 Memory Block

7.2 Tags

This block takes in the signal from part of the MATLAB simulation and transmits it to the other part of the simulation. The use of wires can be reduced and gives a better understanding of the circuits. The “from” tag takes in the signal and the “goto” tag sent the received signal.

www.manaraa.com

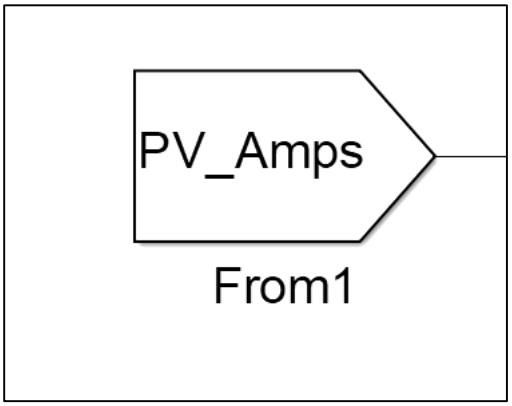

Figure 7.2 From Tag

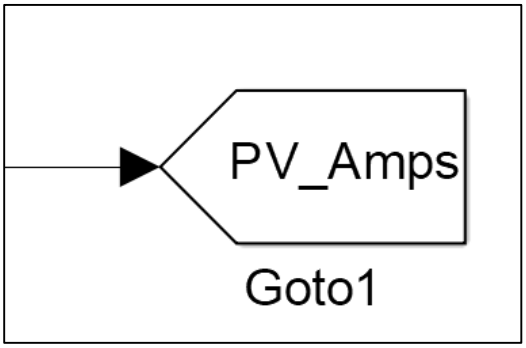

Figure 7.3 Goto Tag

7.3 Switch

The switch is like a logic device. It takes in two input signal and one condition input. Based on the given condition, the output delivers one of the input signals. The switch sends a signal through input-1 if input-2 satisfies, otherwise sent the signal through input-3. This block has three inputs. The first and third are data inputs, while the second one is the control port.

www.manaraa.com

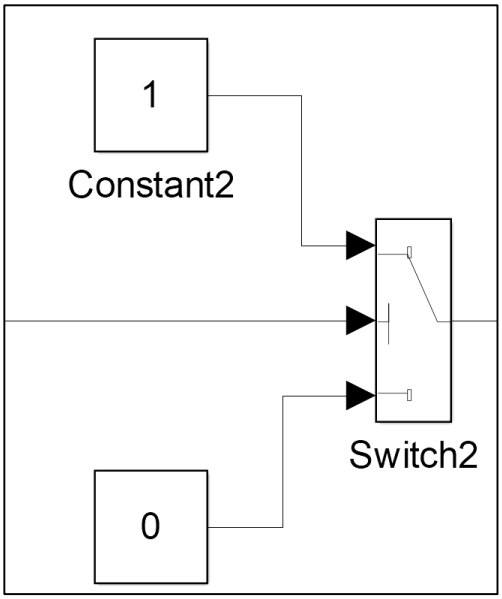

Figure 7.4 Switch Block

7.4 First-Order Filter

The first-order filter takes in the input and returns a filtered output signal. The transfer function working inside the block is different for low and high pass filter. For the low pass filter, the equation goes like as follows:

$$H(s) = \frac{1}{1 + Ts} \quad (7.1)$$

The equation for the high pass filter is given as follows:

$$H(s) = \frac{Ts}{1 + Ts} \quad (7.2)$$

In the above equations, T is the time constant, while s is the Laplace operator.

www.manaraa.com

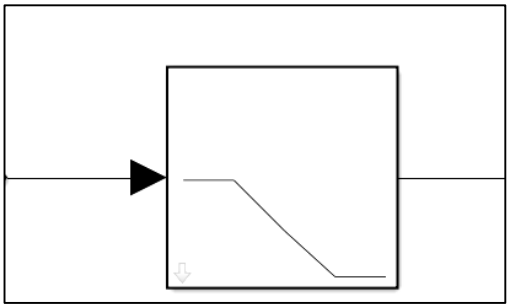

Figure 7.5 First-Order Filter Block

7.5 Second-Order Filter

The second-order filter takes in the input and returns a filtered output signal. This filter can work both with AC and DC signal. The transfer function working inside the block can define the functionality of the filter type. The following transfer functions define the various modes of operations:

For a low-pass filter:

$$H(s) = \frac{\omega_n^2}{s^2 + 2\zeta\omega_n s + \omega_n^2} \quad (7.3)$$

For a high pass filter:

$$H(s) = \frac{s^2}{s^2 + 2\zeta\omega_n s + \omega_n^2} \quad (7.4)$$

For a band pass filter:

$$H(s) = \frac{2\zeta\omega_n}{s^2 + 2\zeta\omega_n s + \omega_n^2} \quad (7.5)$$

For a band stop filter:

$$H(s) = \frac{s^2 + \omega_n^2}{s^2 + 2\zeta\omega_n s + \omega_n^2} \quad (7.6)$$

www.manaraa.com

From the above equations, s is the Laplace operator, ς is the damping coefficient and ω_n is the natural frequency and is given by $\omega_n = 2 * pi * f$.

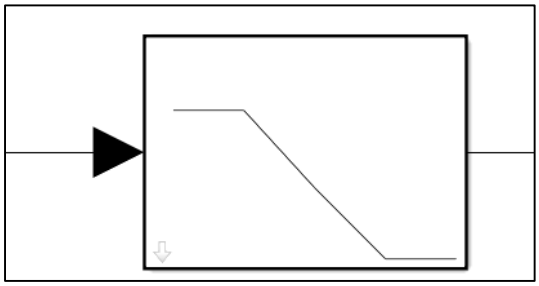

Figure 7.6 Second-Order Filter Block

www.manaraa.com

CHAPTER 8: 13-BUS DISTRIBUTION FEEDER

The main purpose is to serve the load. This is done by creating a small grid system to transmit and distribute the power to the various load. The 13-bus system shown is a single line diagram of a radial network, having 13 buses, 11 lines and 8 loads. The loads are created by using impedances. First, the voltage is stepped up from 1KV to 115KV and then it was stepped down to 4.16KV and distributed throughout the system.

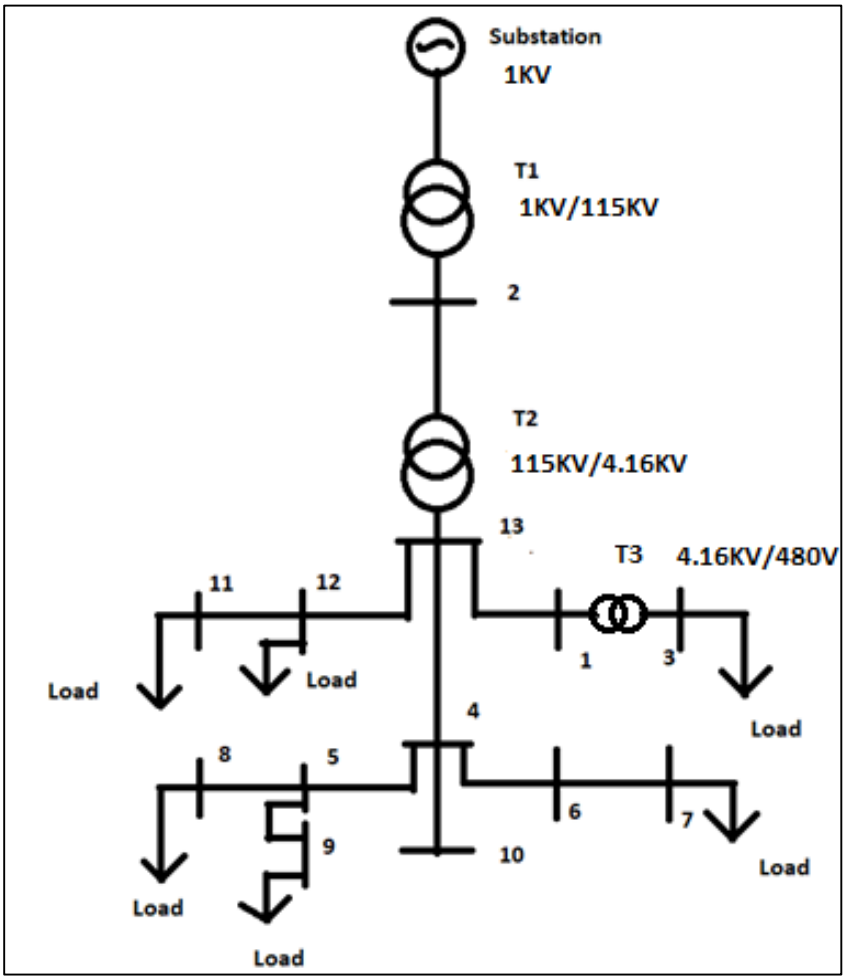

Figure 8.1 13 Bus Radial Network

www.manaraa.com

CHAPTER 9: RESULTS

This project highlights a micro-grid system with photo-voltaic system, fuel cell, and a doubly fed induction generator. Each system provides individual power to an infinite bus with a constant 60 Hz frequency and a voltage of 690 V (line-to-line). The simulation is run for 0.5 seconds. The three systems are in synchronism with each other. For 0.4 to 0.6 seconds, the irradiance is reduced, to find out that the battery can provide the back-up. During the low irradiance phase, the input voltage and current reduce. [9]

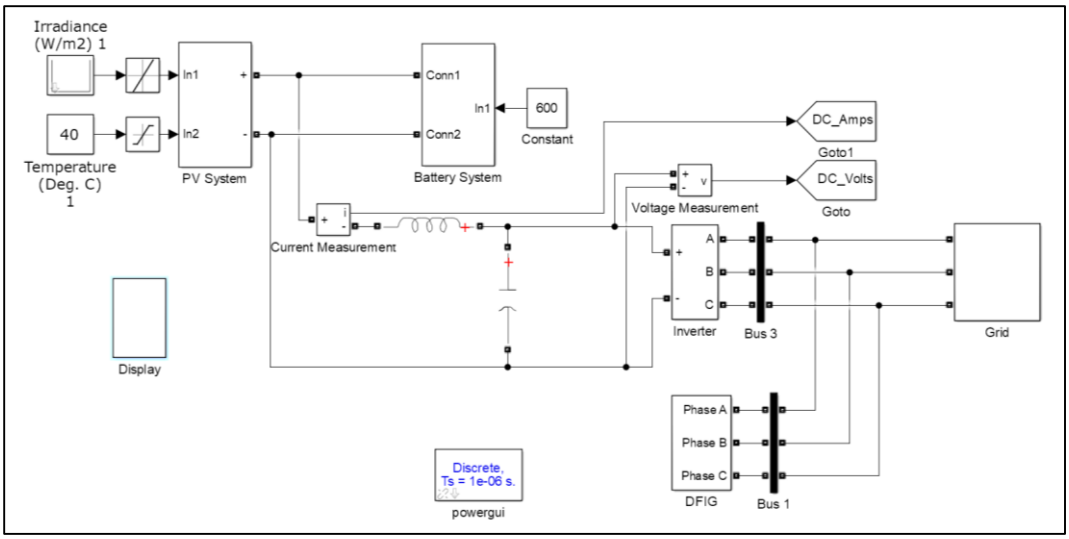

Figure 9.1 Circuit Diagram of Simulink Model

The DFIG is the major source of power here. In case the whole DC system fails, the generator can alone provide power to the grid. The DFIG is called doubly-fed because it has two sources of input. The rotor has to be fed with three-phase AC power at 60 Hz, to produce a synchronously rotating magnetic field. This will induce the stator to link up with the magnetic field of the rotor to create its own rotating magnetic field [6].

www.manaraa.com

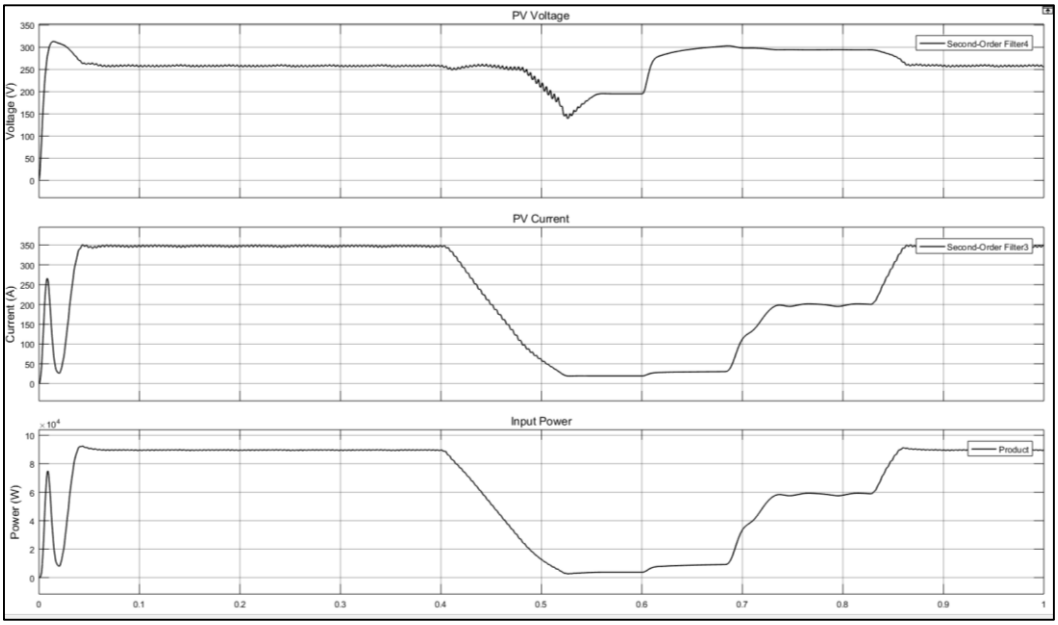

Figure 9.2 Output from Photovoltaic Cell

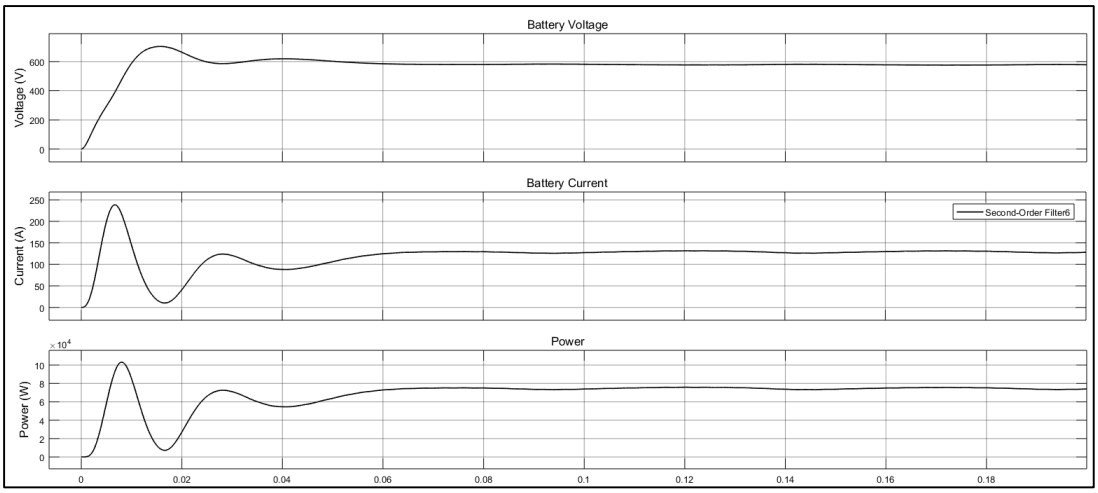

Figure 9.3 Output from Battery System

Now when torque is applied to the rotor, it produces a mechanical rotation and hence the creates a difference in magnetic linkages between the rotor and the stator. Hence current is produced in the stator and three phase supply is obtained at the stator terminals. The battery keeps the output constant, so there are no interruptions in the output. The inverter converts DC input to a stable three-phase output. In the case of the DC system interruption, the DFIG takes over and supplies output to the whole system.

www.manaraa.com

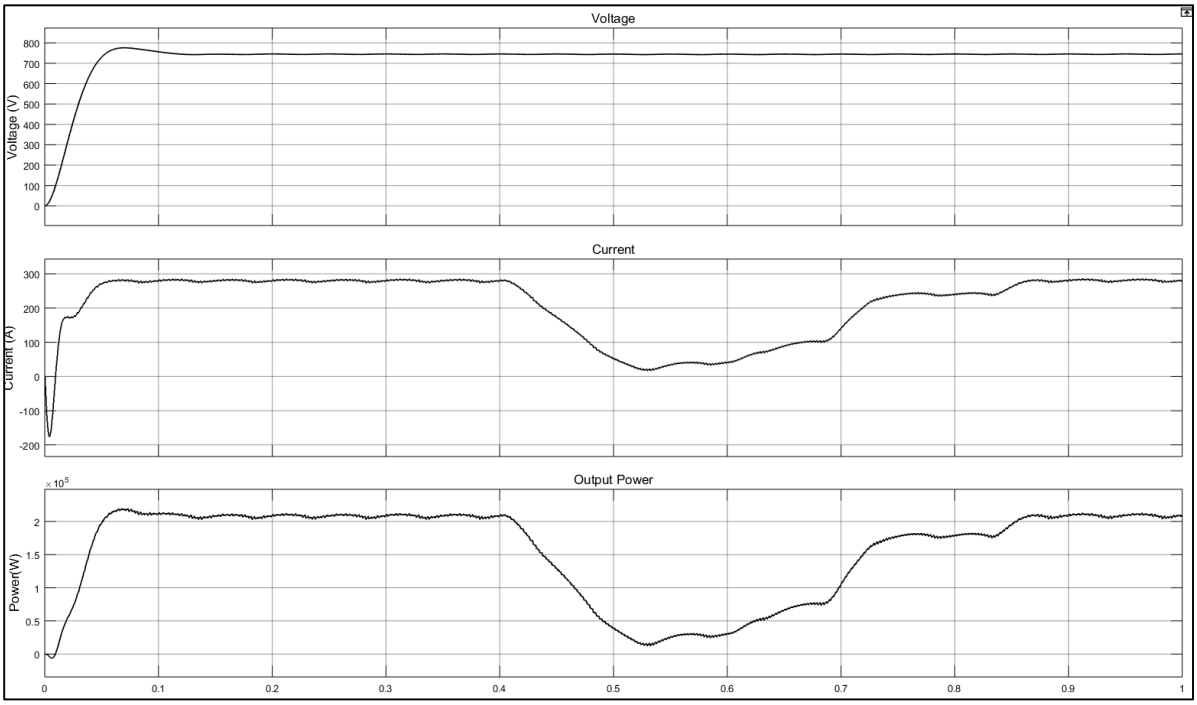

Figure 9.4 DC Output

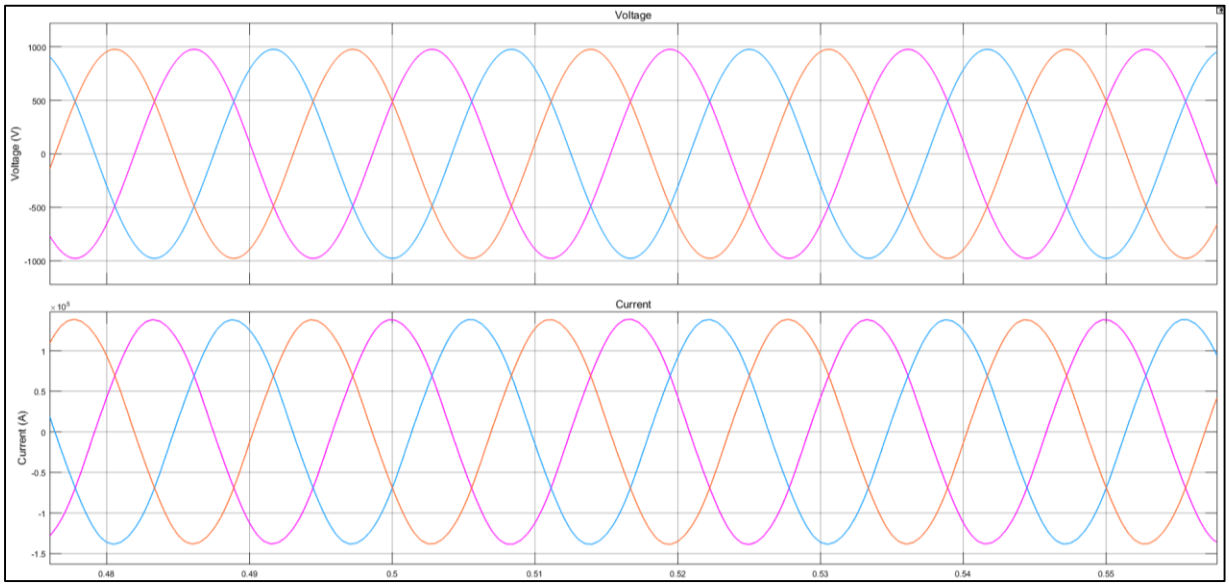

Figure 9.5 Three-Phase AC Output

www.manaraa.com

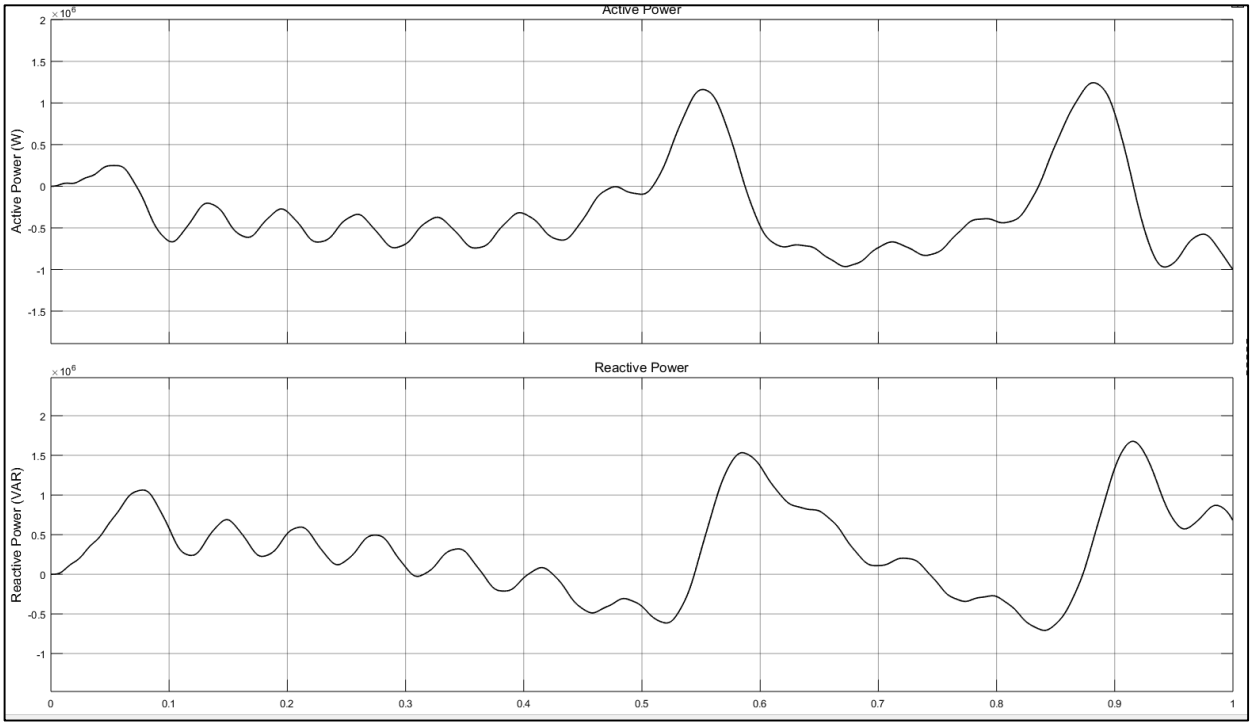

Figure 9.6 Flow of Active and Reactive Power

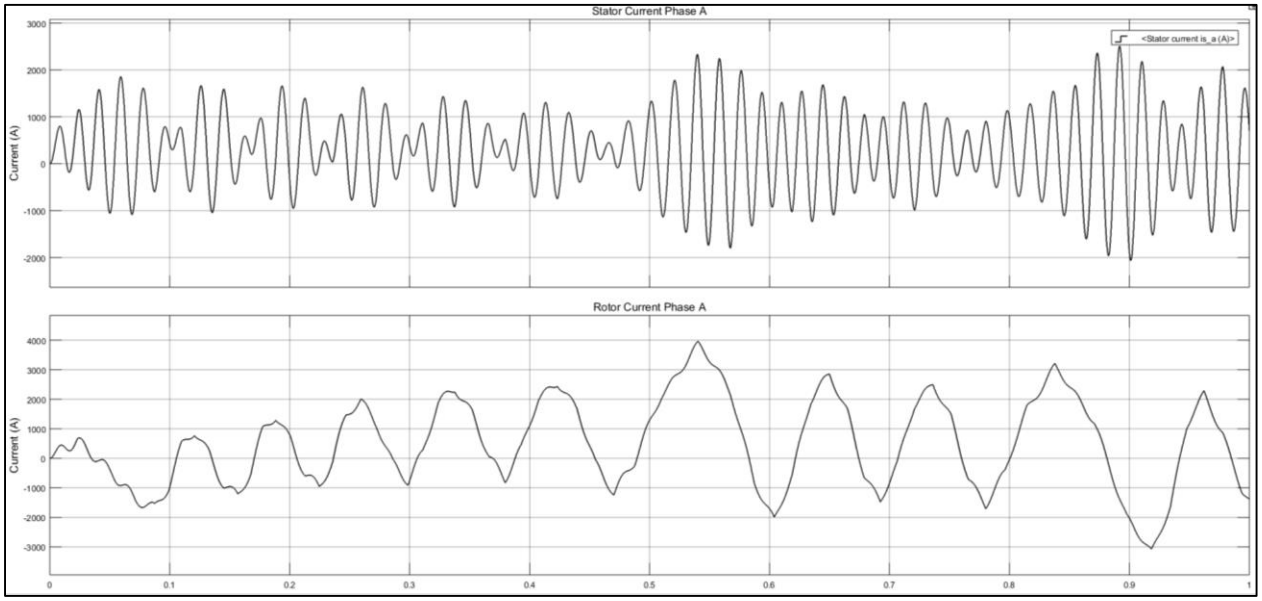

Figure 9.7 Stator and Rotor Current

www.manaraa.com

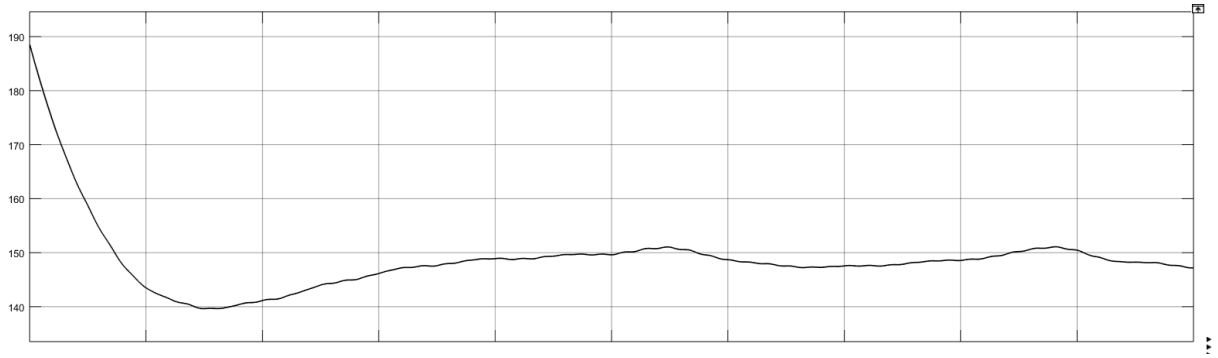

Figure 9.8 DFIG Angular Speed

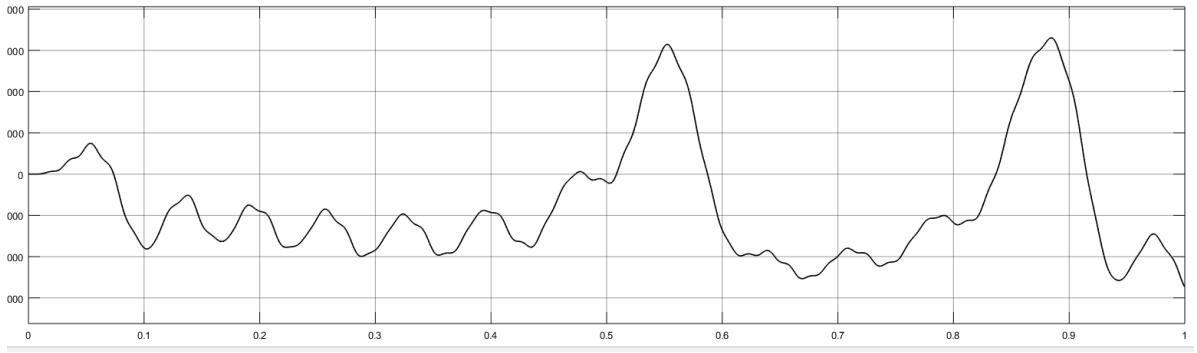

Figure 9.9 Torque

www.manaraa.com

CHAPTER 10: CONCLUSION

This paper provides an insight on how the use of a hybrid system helps in improving power quality and efficiency of the system. The application of PV cell, wind, natural gas and fuel cell all together has its own advantages, but so many devices integrated together will only add to the cost and increase the harmonics in the system [10]. Simulation of fuel cell alone is a big risk, as we have to operate the cell in charging and discharge cycle, which will lead to temporary disoperation of the fuel cell [12]. Using of Photovoltaics alone will be insufficient as change of irradiance changes the performance of the curve [15]. Single phase power conditioning will be easy, but will increase the cost as we need three duplicate systems with synchronous check to implement the whole power plant [16]. The integration of wind generator along PV cell and battery system will enhance the quality of power and the extra active power will result in boosting up of voltage. This has its own advantage. The losses in the system will reduce the power, but the extra flow of active power will feed in the gap in the system and hence we can cater to the losses in the system, thus improving efficiency, better performance of the system and improve power quality on load side [17].

The efficiency of the PV system working alone can only provide 20-30% efficiency. But with the inclusion of DFIG the overall system efficiency has increased, thus making the system more reliable. The system gives uninterrupted voltage with no abnormalities. The power given by the PV system is 136 KW. The power provided by the battery system is 81.56 KW. The total DC output power at the inverter end is 198.6 KW. So the efficiency of the DC system is 91.28%. The

www.manaraa.com

efficiency of DFIG is approximately 85%. Hence the overall efficiency of the system is 77.59%. The cost of a SunPower PV cell costs around 14,000$-30,000$. The price quote of a 600V battery system is around 1000$. The cost of Schneider Electric 1kV three-phase inverter is around 14,000$ and the price quote of a 2MW wind turbine is approximately $2.8 million. So the overall cost of the system is around $ 2.9 million. An output voltage of 1KV line-to-line is produced line current of 138 KA is produced.

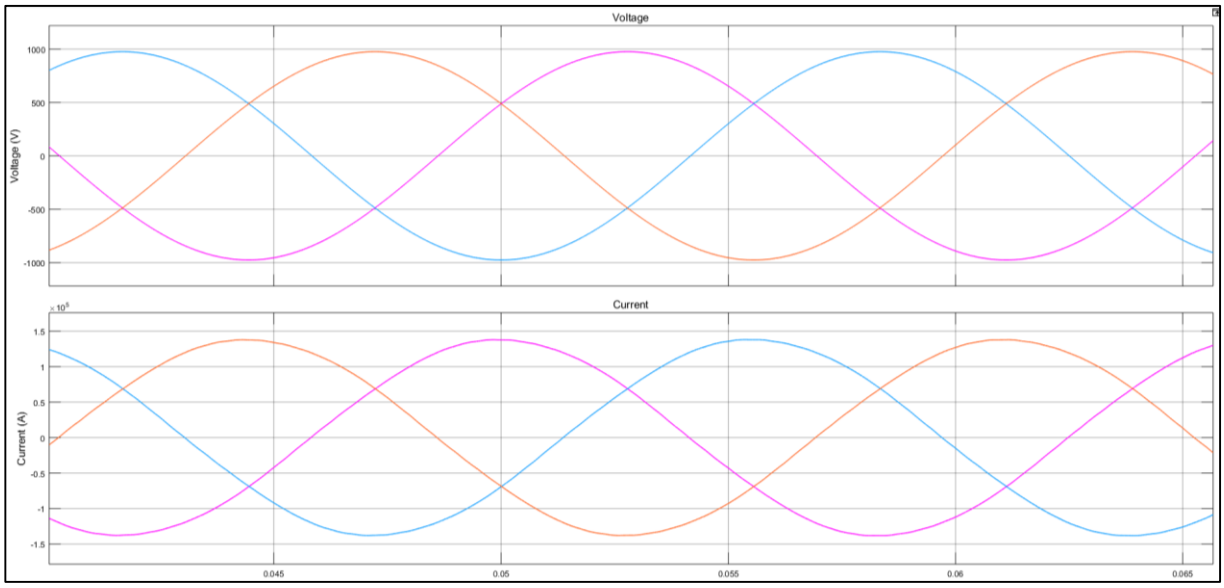

Figure 10.1 Three-Phase AC Output

www.manaraa.com

REFERENCES

[1] C. Zhu, L. Fan and M. Hu, "Modeling and Simulation of a DFIG-Based Wind Turbine for SSR," 41st North American Power Symposium, 2009.

[2] L. Fan, R. Kavasseri and Z. L. Miao, "Modeling of DFIG-Based Wind Farms for SSR Analysis," *IEEE Transactions On Power Delivery,* 2010.

[3] IEEE Committee Report, "First benchmark model for computer simulation of subsynchronous resonance," *IEEE Trans. Power and Apparatus Systems,* vol. 96, no. 5, p. 15651672, Sep./Oct. 1977.

[4] "Modeling and Stability Analysis of a DFIG-Based Wind-Power Generator Interfaced with a Series-Compensated Line," *IEEE Transactions On Power Delivery,* vol. 24, no. 3, 2009.

[5] L. Qu and W. Qiao, "Constant Power Control of DFIG Wind Turbines with Supercapacitor Energy Storage," *IEEE Transactions On Industry Applications,* vol. 47, no. 1, January/February 2011.

[6] M. K. Döş_ogˇlu and A. B. Arsoy, "Transient modeling and analysis of a DFIG based wind farm with supercapacitor energy storage," *Electrical Power and Energy Systems,* vol. 78, p. 414–421, 2016.

[7] Z. Jiang and X. Yu, "Modeling and Control of an Integrated Wind Power Generation and Energy Storage System," *National Science Foundation under grants,* Vols. ECCS-0652300, ECCS-0748032 and ECCS-0821126. .

[8] H. Keyhani and H. A. Toliyat, "A new generation of buck-boost resonant AC-link DC-DC converter," *2013 Twenty-Eighth Annual IEEE Applied Power Electronics Conference and Exposition (APEC),* 2013.

[9] S. Adhikari and F. Li, "Coordinated V-f and P-Q Control of Solar Photovoltaic Generators With MPPT and Battery Storage in Microgrids," *IEEE Transactions on Smart Grid Year,* pp. Volume: 5, Issue: 3, 2014.

www.manaraa.com

[10] J.-S. Lai, "Power Conditioning Systems for Renewable Energies," *Proceeding of International Conference on Electrical Machines and Systems,* 8-11 October 2007.

[11] J. Spanicek and D. Platt, "Minimal Circuit For Power System Conditioning," *Proceedings of 1995 International Conference on Power Electronics and Drive Systems. PEDS 95.*

[12] M. Mwinga, B. Groenewald and M. McPherson, "Design, Modelling and Simulation of a Fuel Cell Power Conditioning System," *Journal of Thermal Engineering, Yildiz Technical University Press,* vol. 1, no. 3, pp. 408-419, May 2015.

[13] K.-s. T. S. Rahman, "System Performance Improvement provided by a Power Conditioning Subsystem for a Central Station Photovoltaic-Fuel Cell Power Plant," *IEEE Transactions on Energy Conversion,* vol. 3, no. 1, March 1988.

[14] S. Patrobers, X. Ai, B. G. Teshager and W. Kunyu, "Modelling and control of a VSC medium-voltage DC distribution network with DFIG wind farm," *The 6th International Conference on Renewable Power Generation,* 19–20 October 2017.

[15] S. Heo, W.-K. Park and I. Lee, "Microgrid Design with Renewable Energy and Storage based on Power Conditioning System for Autonomous Island Operation," *Electronics and Telecommunications Research Institute.*

[16] S. Heo, W.-K. Park and I. Lee, "Single-phase Power Conditioning System with Slew-Rate Controlled Synchronizer for Renewable Energy System in Microgrid," *5th International Conference on Renewable Energy Research and Applications,* pp. 20-23, November 2016.

[17] D. L. H. Aik and G. Andersson, "Impact of Renewable Energy Sources on Steady-state Stability of Weak AC/DC Systems," *CSEE Journal of Power and Energy Systems,* vol. 3, no. 4, December 2017.

www.manaraa.com

APPENDIX A: RATING OF SYSTEM

Table A.1 Rating of Doubly Fed Induction Generator

Power	2 MW
Voltage(L-L)	690 V
Frequency	60 Hz
Stator Resistance	2.59 mΩ
Rotor Resistance	2.89 mΩ
Stator Inductance	2.586 mH
Rotor Inductance	2.586 mH
Mutual Inductance	2.5 mH
Inertia	128 J
Friction Factor	1 mF
Pole Pairs	2

www.manaraa.com

Table A.2 Rating of a PV Array

Power	315.072 W
Open Circuit Voltage	64.6 V
Voltage at Maximum power point	54.7 V
Current at Maximum Power Point	5.76 A
Short Circuit Current	6.14 A

Table A.3 Rating of a Battery

Type	Lithium-Ion
Nominal Voltage	600V
Rated Capacity	6.5 Ah
State of Charge	100%

www.manaraa.com